

# The Lunar and Solar Daily Geomagnetic Variations at Kakioka, Japan, 1913-1976

by

Masanori SHIRAKI

Kakioka Magnetic Observatory  
Kakioka 595, Ibarakiken 315-01, Japan

## Abstract

Hourly values of declination, horizontal intensity and vertical intensity of the geomagnetic field at Kakioka for the period 1913–1976 have been analysed to determine their lunar and solar daily variations, by dividing these data in several ways according to season, sunspot number and magnetic activity. The results are tabulated by the first four harmonic coefficients determined by the Chapman-Miller method and are illustrated by daygraphs, vector diagrams and harmonic dials. Some characteristic points of the results are described and discussed.

## 1. Introduction

The purpose of the present study is to determine the lunar and solar daily variations of the geomagnetic field at Kakioka, Japan, using the hourly data of three elements for the period 1913–1976.

At present the producing mechanism of the lunar and solar daily geomagnetic variations (denoted by  $L$  and  $S$ , respectively) is interpreted by the ionospheric dynamo theory. In this theory these variations are considered to result mainly from electric currents generated by the dynamo action in the ionosphere. This dynamo is powered by the movements of the ionosphere, probably of tidal origin, across lines of force of the Earth's main magnetic field. Tidal movements responsible for  $L$  is considered to be purely of gravitational origin and those responsible for  $S$  to be mainly of thermal origin.

For the study of the ionospheric dynamo theory,  $L$  is more useful than  $S$ , when the observational results are compared with the theoretical ones. This is because the lunar tidal wind system is much simpler than the solar one and the period of lunar tide is incommensurable with that of ionospheric conductivity change. However, as the observed amplitude of  $L$  is much smaller than that of  $S$  (about a tenth) and the period of  $L$  differs so little from that of  $S$  (51 minutes of time), reliable determination of  $L$  requires data ranging over a long period, especially for the studies on the detailed

features of  $L$ .

Up to this time, extensive studies of  $L$  at individual observatories from long-term data have been carried out by a few workers: for example, at Greenwich by Chapman (1957), at Greenwich and Abinger by Leaton *et al.* (1962), at San Fernando by Chapman and Fogle (1968), at Watheroo by Green and Malin (1971) and at Sodankylä by Gupta (1973). But the distribution in latitude and longitude of the observatories is not good enough as yet. So the analysis of  $L$  at Japanese observatories may make great contributions to the understanding of  $L$ .

The former analysis of  $L$  at Kakioka made by the present author (Shiraki, 1977, 1978) using data for 16 years (1958–1973), together with those at Memambetsu and Kanoya for the same period, produced many interesting results of  $L$  in Japan, especially on the seasonal change. To get a better understanding, however, a more precise determination of  $L$  using a much longer term of data is required. For this purpose, all the 57-year data at Kakioka available at present are analysed in the present paper. These data are divided in several ways according to season, sunspot number and magnetic activity and the  $L$  and  $S$  variations are determined by the Chapman-Miller method for each of division. The results are tabulated by the first four harmonic coefficients and are illustrated by the harmonic dials, daygraphs and vector diagrams. Some characteristic points of the results are described and discussed. Detailed interpretations of the results for  $L$  are given in another paper (Shiraki, 1979), in comparison with those results at Memambetsu, Kanoya and 23 other observatories of the world.

## 2. Data

The geomagnetic observatory at Kakioka was established by the Central Meteorological Observatory (now the Japan Meteorological Agency) in 1913, to replace the observatory at Tokyo ( $35^{\circ}41'N$ ,  $139^{\circ}45'E$ ). This was because the latter came to be affected seriously by strong artificial disturbances from electric railways and factories nearby. Kakioka is situated on a gently rolling farm field at a distance of 70 km to the northeast of Tokyo. The geographic and geomagnetic coordinates of the observatory are given in Table 1. A magnetic survey of this area indicates that it is free from the local anomaly. The artificial interference at the site of the observatory is small enough for the practical geomagnetic observation.

The data used in this analysis are hourly values of magnetic declination  $D$ , horizontal intensity  $H$  and vertical intensity  $Z$  for the years 1913–1916 and 1924–1976. No data are available for the years 1917–1923, owing to the loss of original magnetograms by the post-earthquake fires of September, 1923. All hourly values

Table 1. Location and mean geomagnetic field.

Geographic	{ latitude	36°14'N	
	{ longitude	140°11'E	
Geomagnetic	{ latitude	26.0°N	
	{ longitude	206.0°	
Dip latitude		30.2°N	
Mean values of geomagnetic elements for the period 1913-1976*	{ Declination <i>D</i>		6°08.2'W
	{ Horizontal intensity <i>H</i>		29954 nT
	{ Vertical intensity <i>Z</i>		34811 nT
	{ Total intensity <i>F</i>		45924 nT
	{ Inclination <i>I</i>		49°17.3'

\* As there exist some gaps in hourly published values due to the changes of the instrument and its housing for the absolute measurement, all hourly values are adjusted to those at the present level.

used have been taken from the yearbooks of the Kakioka Magnetic Observatory. The changes of the annual mean values of *D*, *H*, and *Z* for the period 1913-1976 are shown in Fig. 1, together with those of *F* (total intensity) and *I* (inclination or dip). The overall means of these elements are given in Table 1.

For the period from 1963 to 1976, the hourly values have been routinely stored in the computer readable magnetic tapes. These tapes are used for the present analysis. The hourly values for the years 1913-1962 were punched on cards from the published tables. The punched data were checked by comparing the daily sums or daily means with the corresponding published values.

The first part of the data (1913-1929) is tabulated in terms of local (135°E meridian time) days, and the latter part (1930-1976) in terms of Greenwich (Universal Time) days. Before the analysis it is necessary to adjust all data to a uniform system. For the subsequent convenience of classification of days according to magnetic activity it was decided to treat all the data in terms of Greenwich days.

On the other hand, until the end of 1954 the hourly values referred to the exact hours of Universal Time and thereafter were means for the interval between successive hours of Universal Time. On this account the data before and after January 1, 1955, were separately treated up to a late stage in the analysis.

For some days data are incomplete. Such days have been omitted from the analysis. Their number is relatively small, being about two percent of the total number of days used. This is the reason why slightly different numbers of days were used for each element.

### 3. Analysis

Periodic variations such as *L* and *S* are adequately represented in the form

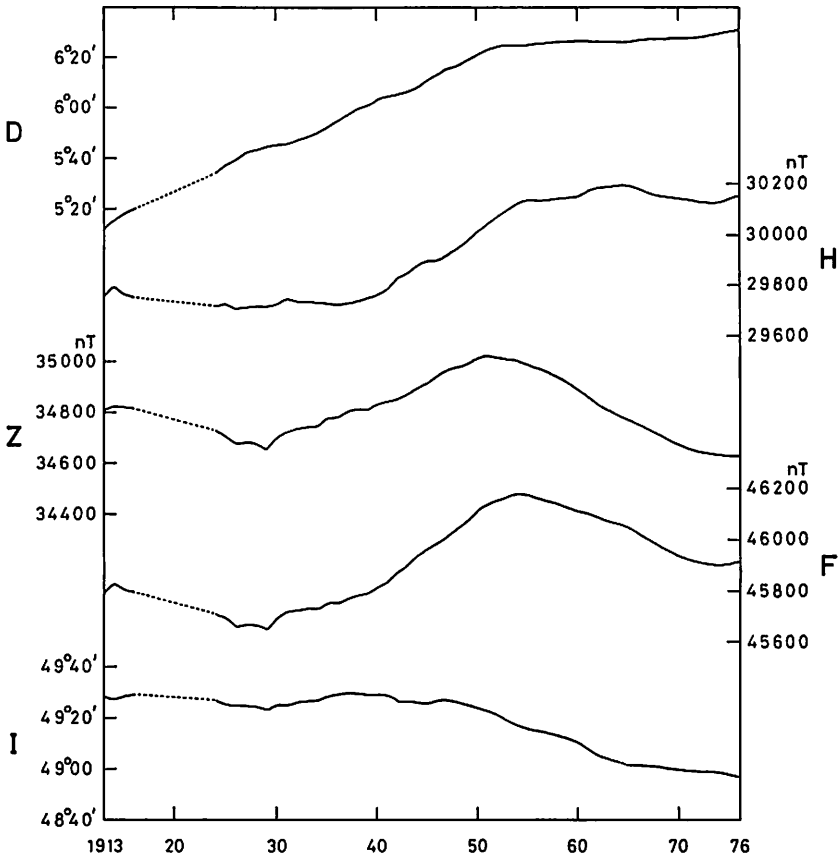


Fig. 1. Secular changes of the declination ( $D$ ), horizontal intensity ( $H$ ), vertical intensity ( $Z$ ), total intensity ( $F$ ), and inclination ( $I$ ) shown by the annual mean values for the period 1913–1976. No values are available for the period 1917–1923, owing to the loss of original magnetograms in the post-earthquake fires of September, 1923. As there exist some gaps in the tabulated annual mean values due to the changes of the instrument and its housing for the absolute measurements, all values are adjusted to those at the present level.

of Fourier coefficients determined by harmonic analysis. If  $l_n$  and  $\lambda_n$  denote the amplitude and phase of the  $n$ -th harmonic of  $L$ , one may write

$$L = \sum L_n = \sum l_n \sin [2\tau + (n-2)t + \lambda_n] \quad (1)$$

Here  $\tau$  denotes the mean lunar time, measured from local lower transit of the mean moon, and  $t$  the mean solar time, measured from midnight.

The harmonic for  $n=2$  has the period of  $M_2$  component in the lunar gravitational potential. And the other harmonics are the results of the combined effects of the tidal

movements of  $M_2$  component with the conductivity changes of ionosphere. The most important harmonic terms are those for which  $n$  is close to 2. And the harmonics for  $n=1, 2, 3$  and 4 are usually determined from the observatory data.

In Eq. (1)  $\tau$  is related to  $t$  by

$$\tau = t - \nu \quad (2)$$

where  $\nu$  is the age of the mean moon: it increases by  $360^\circ$  in one lunation (or synodic month), *i.e.*, in 29.53 mean solar days. Therefore, Eq. (1) is rewritten as follows:

$$L = \sum L_n = \sum l_n \sin (nt - 2\nu + \lambda_n) \quad (3)$$

The expression (3) for  $L$  can also be written as

$$L = a_2(t) \cos 2\nu + b_2(t) \sin 2\nu \quad (4)$$

or

$$L = m_2(t) \sin [2\nu + \mu_2(t)] \quad (5)$$

where

$$a_2(t) = \sum l_n \sin (nt + \lambda_n) = m_2(t) \sin \mu_2(t) \quad (6)$$

$$b_2(t) = \sum l_n \cos (nt + \lambda_n) = m_2(t) \cos \mu_2(t) \quad (7)$$

and  $m_2(t)$  and  $\mu_2(t)$  are the amplitude and phase of the semi-monthly lunar variation, with  $t$  referring to a particular solar hour. A detailed discussion of Eqs. (1)–(7) has been given by Chapman (1957).

On the other hand, if  $s_n$  and  $\sigma_n$  denote the amplitude and phase of the  $n$ -th harmonic of  $S$ , one may write

$$S = \sum S_n = \sum s_n \sin (nt + \sigma_n) \quad (8)$$

Customarily,  $S$  is represented by the first four harmonics for  $n=1, 2, 3$  and 4.

The method of analysis used to determine  $L_n$  and  $S_n$  is that of Chapman and Miller (1940). This method has been used in most of the recent analyses of  $L$  and  $S$  with a large amount of data. The Chapman-Miller method was primarily developed to determine  $L_n$  from observatory data, but it is such a convenient method that  $S_n$  can also be determined as a byproduct. Details of this method were discussed by Tschu (1949), Leaton *et al.* (1962) and Malin and Chapman (1970).

Examination of errors should not be omitted from the analysis of  $L$ . It is usually given by the vector probable error. This represents the radius of a circle centered at the end of the mean vector which contains half the end-points of observed vectors. In the present analysis it was determined by the method described by Malin and Chapman (1970).

#### 4. Results of the analysis

The data for each element were first analysed as a whole, and re-analysed after

Table 2L. Harmonic components of  $L$ . The unit is 0.01  $nT$  for  $l_n$  and  $p.e.$ , degrees for  $\lambda_n$ .

	No. of days	$l_1$	$p.e.$	$\lambda_1$	$l_2$	$p.e.$	$\lambda_2$	$l_3$	$p.e.$	$\lambda_3$	$l_4$	$p.e.$	$\lambda_4$
Declination $D$													
all	20398	34	5	111	99	2	295	46	2	106	15	1	291
winter	6703	42	6	236	120	5	16	49	3	215	14	2	31
equinox	6837	42	11	105	103	4	283	59	4	97	33	2	267
summer	6858	90	7	91	200	5	268	102	5	85	16	3	290
low	6730	33	7	100	89	4	293	39	3	103	16	2	289
medium	6820	33	7	117	101	3	295	45	3	108	15	2	300
high	6848	36	9	117	107	5	298	55	4	107	13	3	282
quiet	3358	58	13	96	110	10	295	51	5	112	10	3	321
medium	6991	46	9	121	106	7	297	55	4	109	16	3	293
disturbed	10049	20	10	87	93	6	294	41	4	103	16	3	283
Horizontal intensity $H$													
all	20385	55	8	231	84	4	72	54	2	236	12	2	77
winter	6714	130	16	282	117	6	109	48	4	268	16	3	90
equinox	6835	51	15	173	65	7	44	54	6	216	18	3	41
summer	6836	79	14	187	108	7	51	70	4	230	10	3	123
low	6722	49	10	235	76	7	74	51	4	234	9	3	49
medium	6818	61	13	220	86	7	75	52	4	236	15	4	84
high	6845	56	16	240	90	7	68	58	5	236	15	4	86
quiet	3348	60	11	238	95	6	71	57	4	246	16	3	88
medium	6992	70	10	239	92	6	66	57	4	239	15	3	71
disturbed	10045	49	13	228	75	7	76	51	5	229	10	4	79
Vertical intensity $Z$													
all	20371	24	5	196	39	2	291	36	1	241	10	2	65
winter	6712	54	6	32	83	4	226	30	3	324	10	2	124
equinox	6813	37	5	206	45	3	314	43	3	231	18	2	38
summer	6846	89	8	202	68	4	347	65	3	223	9	3	64
low	6747	22	4	194	40	4	285	33	2	240	9	2	50
medium	6771	28	6	204	35	4	291	36	3	241	12	2	70
high	6853	24	7	191	41	4	297	39	3	244	10	3	70
quiet	3358	22	7	191	33	4	294	38	3	252	11	2	91
medium	6983	22	7	195	39	4	300	36	3	240	12	2	66
disturbed	10030	24	6	199	40	4	287	36	3	239	9	3	55

subdivision according to season, sunspot number and magnetic activity. In addition, each seasonal division has been subdivided according to month, sunspot number and magnetic activity. Moreover, each division for magnetic activity has also been subdivided according to sunspot number.

Seasonal subdivisions, which were introduced by Lloyd and are now customarily used in dealing with  $L$  and  $S$ , are as follows:

winter ( $w$ ): January, February, November and December

equinox ( $e$ ): March, April, September and October

Table 2S. Harmonic components of  $S$ . The unit is  $0.1 nT$  for  $s_n$ , degrees for  $\sigma_n$ .

	No. of days	$s_1$	$\sigma_1$	$s_2$	$\sigma_2$	$s_3$	$\sigma_3$	$s_4$	$\sigma_4$
<b>Declination <math>D</math></b>									
all	20398	117	28	93	216	60	35	19	228
winter	6703	40	35	38	202	46	21	28	208
equinox	6837	127	31	93	212	74	31	29	227
summer	6858	182	25	149	222	62	49	10	317
low	6730	96	36	80	224	52	39	17	230
medium	6820	111	32	90	219	57	36	18	229
high	6848	144	21	111	209	70	31	21	225
quiet	3358	100	17	99	212	66	33	20	227
medium	6991	109	22	96	215	63	35	19	229
disturbed	10049	130	35	89	219	55	35	18	228
<b>Horizontal intensity <math>H</math></b>									
all	20385	7	100	51	345	35	157	9	1
winter	6714	27	338	30	311	24	119	11	327
equinox	6835	18	103	69	342	48	157	17	354
summer	6836	28	151	63	4	39	179	8	78
low	6722	4	70	42	349	29	157	8	359
medium	6818	7	129	53	350	34	161	10	5
high	6845	12	93	60	337	40	153	10	358
quiet	3348	35	160	53	338	36	158	10	4
medium	6992	22	148	51	340	35	158	10	3
disturbed	10045	22	6	51	350	34	156	8	357
<b>Vertical intensity <math>Z</math></b>									
all	20371	72	88	38	318	32	160	11	354
winter	6712	55	75	31	302	28	137	15	327
equinox	6813	75	88	41	318	39	158	18	349
summer	6846	87	97	44	328	34	183	8	62
low	6747	54	90	30	326	28	164	10	352
medium	6771	67	90	35	320	30	161	11	355
high	6853	94	86	49	311	37	157	13	354
quiet	3358	62	89	43	314	34	158	12	354
medium	6983	66	89	41	315	33	159	12	354
disturbed	10030	79	88	34	322	31	162	11	353

summer ( $s$ ): May, June, July and August

In the subdivision according to sunspot number, the data were classified into three divisions by the annual mean Zürich sunspot number  $R$ :

low ( $l$ ): 1913–1914, 1924, 1931–1934, 1942–1945, 1952–1954, 1963–1965, 1975–1976

medium ( $m$ ): 1915–1916, 1925–1927, 1929–1930, 1935, 1940–1941, 1951, 1955, 1961–1962, 1966, 1971–1974

high ( $h$ ): 1928, 1936–1939, 1946–1950, 1956–1960, 1967–1970

The boundary values of  $R$  between divisions were chosen so that the data might be

Table 3L. Harmonic components of  $L$ . The unit is  $0.01 nT$  for  $l_n$  and  $p.e.$ , degrees for  $\lambda_n$ .

	No. of days	$l_1$	$p.e.$	$\lambda_1$	$l_2$	$p.e.$	$\lambda_2$	$l_3$	$p.e.$	$\lambda_3$	$l_4$	$p.e.$	$\lambda_4$
Declination $D$													
January	1707	85	14	256	178	8	42	85	6	237	26	4	53
February	1565	66	16	209	127	9	9	47	6	184	5	4	286
March	1731	16	24	133	44	9	259	45	7	54	30	5	243
April	1694	38	22	32	94	11	246	60	9	56	41	6	253
May	1737	55	18	59	160	10	254	100	9	68	29	6	264
June	1680	102	16	86	191	11	256	94	7	72	11	6	258
July	1723	100	19	107	228	10	273	102	8	91	11	6	347
August	1718	116	16	96	236	12	281	127	9	104	23	6	314
September	1680	104	18	115	217	11	295	126	8	122	41	6	290
October	1731	41	18	124	92	9	302	47	6	119	28	5	283
November	1691	17	11	101	88	7	330	34	6	164	19	4	348
December	1740	40	11	250	129	8	18	57	5	234	19	4	55
Horizontal intensity $H$													
January	1705	193	26	310	158	10	124	62	8	289	15	6	121
February	1576	124	31	258	125	12	110	55	9	261	17	7	87
March	1729	76	28	143	33	14	21	47	11	205	25	7	25
April	1691	68	36	111	33	14	32	50	10	217	14	6	34
May	1737	88	23	185	86	14	52	67	8	226	13	6	115
June	1663	92	21	183	110	12	57	72	7	233	13	5	207
July	1720	58	32	183	108	14	61	62	6	237	17	6	128
August	1715	82	22	198	140	15	38	83	8	224	16	6	67
September	1677	85	29	218	112	12	48	74	9	231	11	7	84
October	1736	53	22	217	84	10	50	48	9	214	24	6	44
November	1678	90	28	243	73	12	76	39	8	240	19	6	76
December	1754	169	26	285	125	11	107	44	6	274	15	7	81
Vertical intensity $Z$													
January	1701	81	10	35	123	5	220	48	5	350	14	4	168
February	1583	47	10	340	72	6	224	31	4	302	8	4	101
March	1728	21	13	269	68	6	285	33	7	219	21	5	35
April	1685	44	13	219	71	9	310	43	6	209	18	4	16
May	1735	57	9	228	62	7	323	55	4	217	9	4	35
June	1679	81	10	200	67	6	332	59	5	220	6	3	17
July	1714	118	16	198	81	8	359	71	6	224	13	5	97
August	1718	105	10	194	77	8	7	75	5	229	14	4	67
September	1675	69	12	208	44	8	18	65	5	245	13	4	46
October	1725	39	9	157	30	6	309	37	6	242	20	4	56
November	1685	37	12	82	49	7	254	26	4	268	16	4	84
December	1743	81	10	34	93	6	223	34	4	343	9	4	145

divided in equal numbers of years (19 years). The mean sunspot numbers for the three divisions are as follows:  $R(l)=15.6$ ,  $R(m)=52.0$ ,  $R(h)=119.3$ . Overall mean is 62.3.

In the subdivision according to magnetic activity, the data were classified again into three divisions by a daily index of magnetic activity:

quiet ( $q$ ): the five quietest days of any particular month

disturbed ( $d$ ): the fifteen most disturbed days of the month

Table 3S. Harmonic components of  $S$ . The unit is  $0.1 nT$  for  $s_n$ , degrees for  $\sigma_n$ .

	No. of days	$s_1$	$\sigma_1$	$s_2$	$\sigma_2$	$s_3$	$\sigma_3$	$s_4$	$\sigma_4$
Declination $D$									
January	1707	36	38	47	201	52	23	32	212
February	1565	56	22	48	187	52	11	28	197
March	1731	116	21	100	187	89	12	38	204
April	1694	159	21	115	202	84	23	28	232
May	1737	173	25	135	223	60	48	11	303
June	1680	191	20	149	218	55	44	10	327
July	1723	188	23	154	218	60	41	6	343
August	1718	178	33	159	231	73	58	14	309
September	1680	148	44	120	242	75	63	25	264
October	1731	96	40	65	217	67	35	35	224
November	1691	48	36	34	211	43	27	27	213
December	1740	27	57	29	217	39	25	26	207
Horizontal intensity $H$									
January	1705	21	5	39	300	29	117	15	330
February	1576	33	332	23	307	20	100	9	308
March	1729	32	56	59	319	44	132	18	322
April	1691	19	155	78	346	60	155	19	350
May	1737	23	176	65	2	45	173	7	54
June	1663	19	152	55	6	40	175	8	79
July	1720	27	146	59	7	35	180	7	88
August	1715	44	141	73	360	38	187	11	86
September	1677	36	130	80	352	50	175	14	23
October	1736	11	55	65	345	45	165	20	4
November	1678	26	343	32	327	25	142	11	348
December	1754	31	324	28	309	25	113	11	314
Vertical intensity $Z$									
January	1701	48	79	35	312	32	145	17	338
February	1583	70	76	36	285	30	121	15	313
March	1728	94	85	56	294	47	131	23	323
April	1685	85	91	48	314	47	155	20	352
May	1735	79	96	42	329	34	181	9	48
June	1679	93	97	45	320	30	183	8	76
July	1714	96	96	47	321	33	178	7	64
August	1718	80	98	46	342	37	190	10	60
September	1675	58	97	42	1	42	193	17	26
October	1725	67	79	32	316	32	157	17	346
November	1685	60	76	31	301	27	140	13	330
December	1743	43	68	26	311	27	141	14	326

medium ( $m$ ): the remaining days of the month

This method of classification was introduced by Leaton *et al.* (1962) to avoid the effect of correlation between magnetic activity and sunspot number. The  $C_i$  index for the years 1913–1916 and 1924–1931 and the  $A_p$  index for the years 1932–1976 were taken as the criterion for selecting the five quietest days and the fifteen most disturbed days of the month. On this basis the mean values of  $C_i$  and  $A_p$  indices

Table 4L. Harmonic components of  $L$ . The unit is  $0.01 nT$  for  $l_n$  and  $p.e.$ , degrees for  $\lambda_n$ .

	No. of days	$l_1$	$p.e.$	$\lambda_1$	$l_2$	$p.e.$	$\lambda_2$	$l_3$	$p.e.$	$\lambda_3$	$l_4$	$p.e.$	$\lambda_4$
Declination $D$													
winter													
low	2182	19	9	239	97	5	12	42	4	218	11	3	15
medium	2258	51	11	235	127	7	17	52	4	216	15	3	31
high	2263	52	11	235	133	8	19	53	5	212	17	5	41
equinox													
low	2267	38	17	71	97	7	273	58	6	88	33	4	268
medium	2286	42	17	119	109	7	285	55	6	96	28	5	268
high	2284	53	20	119	103	9	289	67	9	106	38	5	265
summer													
low	2281	82	11	101	167	9	271	82	5	88	16	4	296
medium	2276	99	13	90	208	8	265	103	7	87	20	4	298
high	2301	89	14	82	224	11	267	122	10	82	12	5	269
Horizontal intensity $H$													
winter													
low	2205	96	18	280	103	9	113	42	6	266	6	4	105
medium	2251	134	19	273	117	10	108	42	6	271	20	5	79
high	2258	162	30	291	131	13	108	58	9	268	21	7	96
equinox													
low	2255	41	20	205	68	11	39	50	6	216	21	6	40
medium	2289	86	28	171	62	15	47	53	8	218	13	6	55
high	2291	38	32	141	66	14	45	59	10	215	22	6	34
summer													
low	2262	64	15	187	95	10	59	70	7	229	4	5	34
medium	2278	61	20	182	113	12	58	70	7	232	14	6	121
high	2296	113	29	190	121	13	39	71	8	228	16	6	139
Vertical intensity $Z$													
winter													
low	2198	48	7	40	82	4	231	25	3	324	3	3	164
medium	2249	46	6	24	78	6	223	28	3	324	12	3	118
high	2265	70	12	33	89	6	225	36	5	325	14	4	122
equinox													
low	2256	25	7	202	47	6	313	39	3	223	17	3	45
medium	2275	44	8	215	42	8	317	45	6	232	17	4	34
high	2282	42	10	200	47	8	311	45	6	236	19	4	36
summer													
low	2293	82	8	204	54	5	338	60	5	226	11	3	43
medium	2247	89	12	199	65	6	347	63	4	223	13	4	78
high	2306	94	11	201	87	7	353	73	5	221	5	5	71

for the three divisions are approximately 0.1, 0.4 and 1.0 for  $Ci$  index and 4, 8 and 23 for  $Ap$  index, respectively. According to the conversion table between  $Ci$  and  $Ap$  indices, the above mean values of  $Ap$  index correspond to those of  $Ci$  index, respectively. Therefore, the later numerical expression of the change of  $L$  and  $S$  with magnetic

Table 4S. Harmonic components of  $S$ . The unit is  $0.1 nT$  for  $s_n$ , degrees for  $\sigma_n$ .

	No. of days	$s_1$	$\sigma_1$	$s_2$	$\sigma_2$	$s_3$	$\sigma_3$	$s_4$	$\sigma_4$
Declination $D$									
winter									
low	2182	28	68	33	218	39	24	24	208
medium	2258	39	43	39	207	45	22	27	298
high	2263	61	17	46	188	54	18	33	207
equinox									
low	2267	105	40	80	222	64	35	27	228
medium	2286	121	35	90	216	71	32	29	228
high	2284	159	22	113	202	88	28	33	225
summer									
low	2281	159	28	124	227	54	53	9	307
medium	2276	175	27	143	224	59	50	10	317
high	2301	212	22	179	218	72	44	11	325
Horizontal intensity $H$									
winter									
low	2205	29	318	22	317	21	115	9	321
medium	2251	25	339	30	314	24	122	12	332
high	2258	30	356	39	305	27	119	13	326
equinox									
low	2255	16	89	56	346	41	158	14	352
medium	2289	18	118	71	346	48	161	17	358
high	2291	22	101	80	335	55	153	18	350
summer									
low	2262	23	138	52	5	34	181	7	68
medium	2278	30	160	67	9	40	183	9	82
high	2296	30	152	71	357	45	173	9	82
Vertical intensity $Z$									
winter									
low	2198	39	68	23	311	25	141	12	326
medium	2249	50	78	29	304	27	137	14	328
high	2265	74	76	41	296	33	135	17	328
equinox									
low	2256	57	92	32	327	34	160	16	347
medium	2275	69	90	37	322	36	159	18	351
high	2282	100	84	54	310	46	154	20	350
summer									
low	2293	70	100	37	333	30	187	8	52
medium	2247	82	98	42	330	32	185	8	60
high	2306	109	94	55	323	39	179	9	71

activity is carried out by using the mean values of  $Ci$  index (see section 5.8.).

As noted above, the data before and after January 1, 1955, were separately analysed and the results for the two periods were averaged in the last stage of analysis, with the weight of the number of days for each period.

The published data for the element  $D$  are expressed in angular measure west.

Table 5L. Harmonic components of  $L$ . The unit is  $0.01 nT$  for  $l_n$  and  $p.e.$ , degrees for  $\lambda_n$ .

	No. of days	$l_1$	$p.e.$	$\lambda_1$	$l_2$	$p.e.$	$\lambda_2$	$l_3$	$p.e.$	$\lambda_3$	$l_4$	$p.e.$	$\lambda_4$
Declination $D$													
winter													
quiet	1118	51	15	257	88	11	31	35	8	222	6	5	21
medium	2248	49	11	239	119	8	21	48	5	210	13	3	17
disturbed	3337	24	13	240	131	8	8	53	6	215	18	4	38
equinox													
quiet	1121	64	20	101	114	19	297	64	13	107	25	6	276
medium	2348	45	13	115	114	9	290	70	7	102	37	4	267
disturbed	3368	34	17	91	97	10	271	52	7	88	33	5	265
summer													
quiet	1119	89	16	96	193	14	270	101	11	89	16	5	306
medium	2395	109	11	101	208	9	269	104	6	87	11	4	306
disturbed	3344	86	15	77	197	10	267	101	7	84	19	4	279
Horizontal intensity $H$													
winter													
quiet	1118	131	22	291	120	11	106	50	7	281	16	4	90
medium	2260	144	15	284	118	9	104	51	5	271	19	4	73
disturbed	3336	134	23	273	113	10	112	46	7	260	15	6	105
equinox													
quiet	1120	53	16	188	70	11	40	54	9	219	24	5	50
medium	2350	45	14	187	68	9	45	51	6	222	16	4	39
disturbed	3365	56	26	164	62	11	43	56	11	212	19	6	40
summer													
quiet	1110	69	23	181	109	13	50	70	8	235	14	4	109
medium	2382	95	19	198	124	8	42	74	6	228	13	5	106
disturbed	3344	65	20	180	102	11	60	67	8	229	8	6	151
Vertical intensity $Z$													
winter													
quiet	1120	67	13	39	87	9	231	26	6	340	7	3	130
medium	2252	62	9	27	80	6	224	31	4	326	11	3	108
disturbed	3340	47	9	27	80	5	228	30	4	317	10	4	135
equinox													
quiet	1121	41	12	239	30	9	322	49	7	243	18	4	57
medium	2343	41	6	219	44	7	322	42	6	230	17	3	35
disturbed	3349	36	9	184	52	6	308	42	7	226	18	4	35
summer													
quiet	1117	81	13	194	70	10	348	63	7	225	12	4	73
medium	2388	82	12	192	79	5	345	66	4	220	12	3	70
disturbed	3341	96	11	208	60	5	350	65	4	225	6	4	49

All phase angles for  $D$  have therefore been corrected by  $180^\circ$  and all amplitudes have been multiplied by a factor so that the results for  $D$  may be expressed in nano Tesla ( $nT$ ) east. The factor used was  $8.713 nT$  per minute of arc, based on the mean values of  $H$  at Kakioka for the period 1913–1976 (see Table 1 and Fig. 1).

The results of the analysis determined from data as a whole are given as "all"

Table 5S. Harmonic components of  $S$ . The unit is  $0.1 nT$  for  $s_n$ , degrees for  $\sigma_n$ .

	No. of days	$s_1$	$\sigma_1$	$s_2$	$\sigma_2$	$s_3$	$\sigma_3$	$s_4$	$\sigma_4$
Declination $D$									
winter									
quiet	1118	36	2	49	194	52	17	29	207
medium	2248	38	17	43	200	48	21	29	208
disturbed	3337	49	53	32	209	43	23	27	207
equinox									
quiet	1121	108	16	103	209	81	30	32	226
medium	2348	115	23	97	210	78	31	30	226
disturbed	3368	146	39	88	216	70	32	28	228
summer									
quiet	1119	158	20	149	220	68	48	11	309
medium	2395	169	23	149	222	66	49	11	315
disturbed	3344	199	28	148	224	56	48	9	321
Horizontal intensity $H$									
winter									
quiet	1118	5	99	35	299	25	120	12	329
medium	2260	11	345	33	303	25	120	11	331
disturbed	3336	48	335	28	321	23	118	10	322
equinox									
quiet	1120	48	156	70	338	50	158	18	357
medium	2350	32	138	68	338	48	156	17	355
disturbed	3365	27	32	69	346	47	158	16	351
summer									
quiet	1110	54	167	65	358	40	182	9	77
medium	2382	45	160	62	360	40	180	9	72
disturbed	3344	12	98	63	8	39	176	8	82
Vertical intensity $Z$									
winter									
quiet	1120	47	80	37	300	31	136	15	328
medium	2252	49	77	34	302	29	137	15	329
disturbed	3340	61	72	27	303	27	138	14	326
equinox									
quiet	1121	65	87	46	314	41	156	19	349
medium	2343	69	87	43	314	40	155	18	348
disturbed	3349	83	88	37	323	37	160	18	350
summer									
quiet	1117	75	96	49	324	35	181	9	58
medium	2388	81	97	47	325	34	182	9	59
disturbed	3341	95	97	42	332	32	185	8	65

in Tables 2( $L, S$ ) and those determined from data for various subdivisions are given for the corresponding headings in Tables 2( $L, S$ )–6( $L, S$ ). Throughout this paper  $L$  is included in the titles of tables and figures that refer only to the  $L$  variation. The same statement is true for  $S$ . Tables 2 $L$ –6 $L$  give the amplitude  $l_n$ , vector probable error  $p.e.$  and phase  $\lambda_n$  of  $L$  harmonics of each element. And Tables 2 $S$ –6 $S$  give

Table 6L. Harmonic components of  $L$ . The unit is  $0.01 nT$  for  $l_n$  and  $p.e.$ , degrees for  $\lambda_n$ .

	No. of days	$l_1$	$p.e.$	$\lambda_1$	$l_2$	$p.e.$	$\lambda_2$	$l_3$	$p.e.$	$\lambda_3$	$l_4$	$p.e.$	$\lambda_4$
Declination $D$													
quiet													
low	1114	71	18	94	113	12	296	57	8	114	14	5	318
medium	1116	68	20	70	110	17	284	48	10	107	14	7	341
high	1128	54	25	124	115	19	304	50	10	113	5	6	273
medium													
low	2306	37	13	107	97	9	294	50	6	102	18	4	285
medium	2340	46	14	147	92	10	301	51	5	114	18	5	293
high	2345	54	14	107	126	11	295	61	6	108	12	5	304
disturbed													
low	3310	23	13	92	77	9	291	27	6	99	16	5	285
medium	3364	24	12	84	109	8	294	41	6	105	15	4	295
high	3375	12	16	108	94	12	299	54	8	104	18	6	274
Horizontal intensity $H$													
quiet													
low	1105	89	18	229	105	10	65	63	8	241	19	6	72
medium	1117	40	17	241	98	12	77	62	8	255	17	5	115
high	1126	57	19	246	87	11	70	47	8	240	15	6	77
medium													
low	2304	73	15	235	89	8	62	53	6	232	9	4	65
medium	2336	72	16	248	93	11	74	56	6	244	17	4	75
high	2352	64	15	236	94	9	62	60	6	241	18	4	71
disturbed													
low	3313	21	18	265	63	11	92	45	6	233	8	5	18
medium	3365	77	23	207	79	12	72	48	8	223	13	7	81
high	3367	61	29	241	88	14	70	62	10	232	14	7	104
Vertical intensity $Z$													
quiet													
low	1116	34	11	221	27	6	296	39	6	254	13	4	85
medium	1114	44	10	166	39	8	307	42	6	247	12	4	96
high	1128	2	11	198	36	8	282	33	7	254	7	5	93
medium													
low	2318	16	10	191	36	5	293	34	4	239	10	3	61
medium	2317	15	8	213	39	6	291	36	4	240	15	3	68
high	2348	32	8	183	44	5	312	39	5	240	12	3	66
disturbed													
low	3313	22	7	179	47	6	280	30	4	234	8	3	24
medium	3340	32	9	219	31	6	291	35	5	239	11	4	65
high	3377	23	10	200	42	7	292	42	6	243	9	4	68

the amplitude  $s_n$  and phase  $\sigma_n$  of  $S$  harmonics of each element. In these tables the unit of  $l_n$  and  $p.e.$  is  $0.01 nT$  and that of  $s_n$  is  $0.1 nT$ . The unit of  $\lambda_n$  and  $\sigma_n$  is degrees. No probable errors are given for  $S$  harmonics, because their probable errors are very small compared with their amplitudes and very close to the probable errors for the corresponding  $L$  harmonics. The total number of days used in the analysis for

Table 6S. Harmonic components of  $S$ . The unit is  $0.1 nT$  for  $s_n$ , degrees for  $\sigma_n$ .

	No. of days	$s_1$	$\sigma_1$	$s_2$	$\sigma_2$	$s_3$	$\sigma_3$	$s_4$	$\sigma_4$
Declination $D$									
quiet									
low	1114	83	23	82	219	56	36	19	227
medium	1116	95	19	97	214	64	35	20	230
high	1128	124	10	119	205	77	29	22	225
medium									
low	2306	90	29	82	223	55	39	18	231
medium	2340	103	24	92	217	60	36	18	230
high	2345	134	16	117	207	74	31	21	226
disturbed									
low	3310	107	43	77	227	48	39	16	230
medium	3364	126	39	87	221	53	36	17	229
high	3375	160	27	105	211	65	32	20	225
Horizontal intensity $H$									
quiet									
low	1105	26	171	43	341	30	158	9	2
medium	1117	37	163	54	343	36	163	11	9
high	1126	42	150	61	332	40	154	11	2
medium									
low	2304	15	159	42	343	30	158	9	2
medium	2336	24	157	52	345	35	162	10	8
high	2352	29	136	60	334	41	153	11	360
disturbed									
low	3313	22	8	41	356	29	156	7	355
medium	3365	18	4	54	355	34	160	9	2
high	3367	25	5	60	342	39	153	9	354
Vertical intensity $Z$									
quiet									
low	1116	47	91	34	320	30	161	12	352
medium	1114	57	92	41	317	32	161	12	357
high	1128	82	86	55	308	40	154	13	354
medium									
low	2318	50	91	33	323	29	163	11	353
medium	2317	62	90	38	317	31	160	11	355
high	2348	87	87	52	309	39	156	13	354
disturbed									
low	3313	60	89	27	330	27	165	10	352
medium	3340	73	89	32	325	29	162	11	354
high	3377	102	85	45	314	36	159	12	353

each division is also included in these tables.

The amplitude  $l_n$  or  $s_n$  is considered to be significant when it exceeds 2.08 times its vector probable error (Leaton *et al.*, 1962). From this viewpoint all  $S$  harmonics are significant, and so are all but 37 of the 588 (4 components  $\times$  3 elements  $\times$  49 subdivisions) harmonics for  $L$ . The insignificant harmonics are those for  $L_1$  (18 of 147)

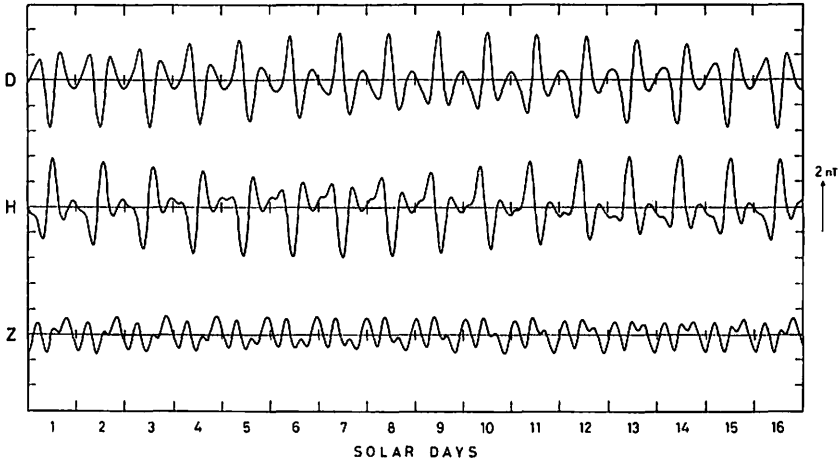


Fig. 2L. Daygraphs for the  $L$  variation for the division "all" in Table 2L. The curves are drawn for 16 solar days (rather more than half a lunation) from the lower transit at new moon.

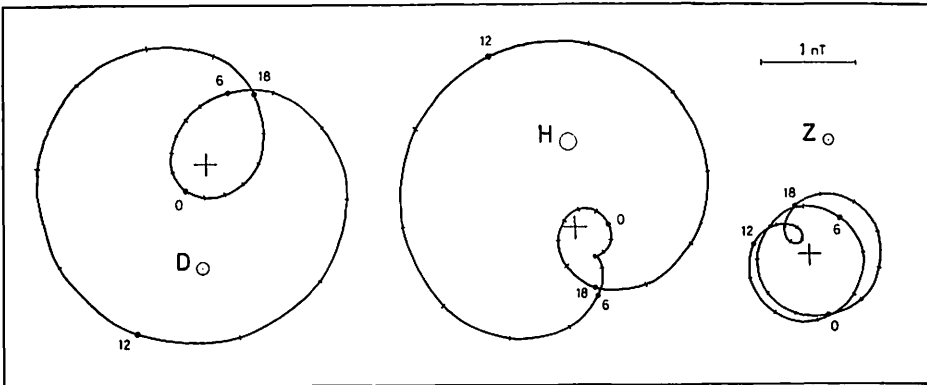


Fig. 3L. Harmonic dials for the half monthly  $L$  variation at particular solar hours, as indicated by the numberings of each six solar hour. The figure corresponds to the  $L$  variation determined from "all" days data. The vector probable error circle is the same as all vectors for an element and is shown beside the name of the element.

and  $L_4$  (19 of 147).

The results of the analysis presented in Tables 2( $L, S$ )-6( $L, S$ ) are illustrated in Figures 5( $L, S$ )-23( $L, S$ ) by the several ways of harmonic dials, daygraphs and vector diagrams. In the harmonic dials, the vector has the length  $l_n$  or  $s_n$ , on the scale shown, and it makes the counterclockwise angle  $\lambda_n$  or  $\sigma_n$  from the righthanded horizontal direction, respectively. The dial vectors are generally not drawn and are indicated only by their end points. For  $L$  the vector probable error circles are gen-

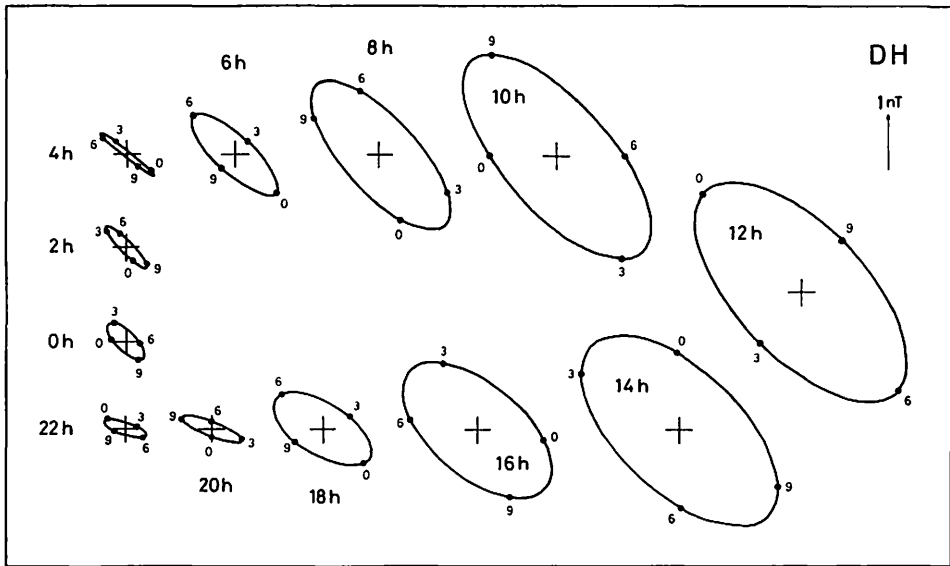


Fig. 4L. Horizontal vector diagrams for the half-monthly  $L$  variation determined from "all" days data. Each vector diagram is an ellipse, corresponding to a particular solar hour, as indicated. This figure includes only the diagrams for the even solar hours, from  $0^{\text{h}}$  to  $22^{\text{h}}$ . The numberings for each ellipse are four lunar phase numbers, where one lunation is composed of 24 lunar phase numbers and the new moon corresponds to number 0.

erally drawn at the end points of vectors.

The daygraphs for  $L$  are drawn from synthetic hourly values calculated from Eq. (1) or (3) with the coefficients given in Tables 2L–6L. Fig. 2L illustrates them for the case of the annual mean  $L$  determined from the entire data ("all" in Table 2L). The curves are drawn for sixteen solar days, slightly more than one half lunation, from the lower lunar transit at new moon. A double daily wave is clearly seen in the figure, but the epochs and the values of maxima and minima change from day to day. However, for convenience of illustration, daygraphs for  $L$  in further figures of this paper are all drawn solely for the epoch of new moon. In synthesizing the 24 hourly values, the change of  $\nu$  in the course of the lunar day is ignored. The daygraphs for  $S$  are drawn from 24 synthetic hourly values calculated from Eq. (8), with the coefficients given in Tables 2S–6S. The time marks for the daygraphs refer to lunar or solar time at intervals of 6 hours.

The vector diagrams are combinations of daygraphs of any two elements: the combination of  $D$  and  $H$  gives the vector diagram in the horizontal plane and that of  $Z$  and either  $D$  or  $H$  gives the vector diagram in the vertical plane. However, as the characteristics seen from the diagrams in the vertical plane are generally

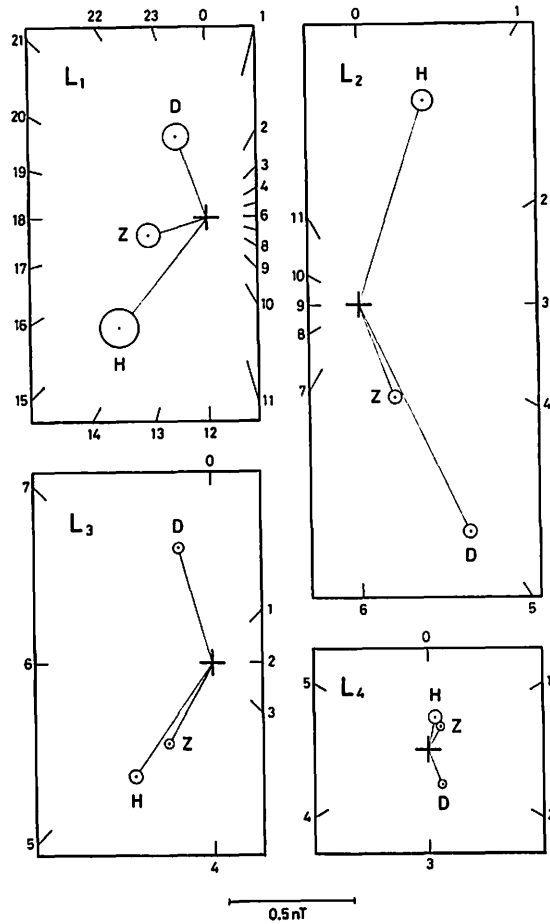


Fig. 5L

common to those from the diagram in the horizontal plane, only the latter is illustrated in this paper except Figs. 6(L, S). Four time marks are given on each curve, and the lunar or solar time at intervals of 6 hours is shown besides.

Generally,  $L$  has been studied as a daily variation, as expressed by Eq. (1) or (3). However, as seen in Eqs. (4)–(7),  $L$  can be expressed in another way so as to undergo a half-monthly variation for any particular solar hour. This is illustrated in Figs. 3L and 4L for the case of the results determined from the whole of the data for 57 years. These figures correspond to Figs. 8 and 7 in Chapman (1957), respectively. In Fig. 3L, each dial point shows the harmonic vector of the half-monthly  $L$  variation with the amplitude  $m_2(t)$  and phase  $\mu_2(t)$  at a particular solar hour  $t$ . Fig. 4L shows the half-monthly horizontal vector diagrams, each of which is an ellipse corresponding to a particular solar hour. Such figures have their own merits for the examination

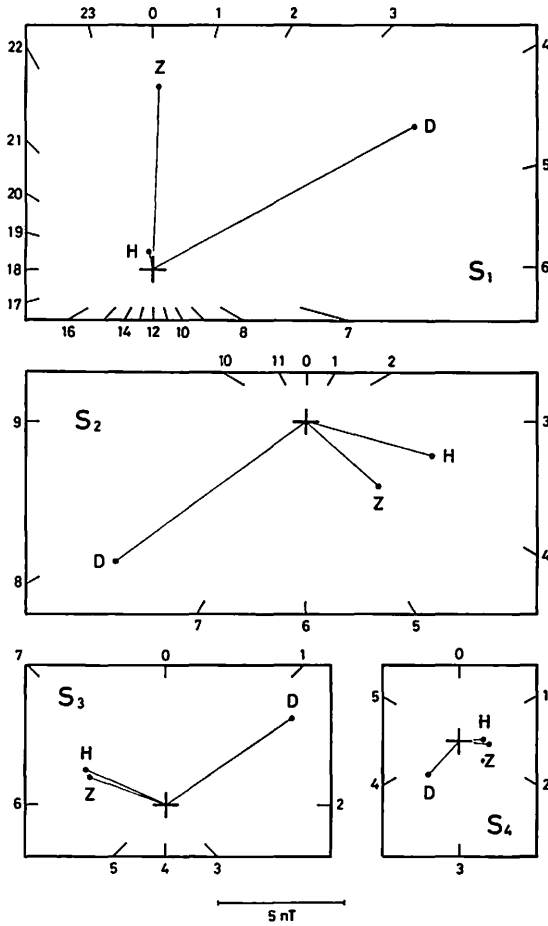


Fig. 5S

Fig. 5(L, S). Harmonic dials for the  $L$  and  $S$  variations for the division "all" in Tables 2(L, S). The numerical suffix indicates the order of the harmonics. The numbering around the rectangle indicates the lunar or solar time at which the maximum of each harmonic occurs. For the  $L$  harmonics the vector probable error circles are drawn at the end points of vectors. The  $L$  vectors are magnified tenfold as compared with the  $S$  vectors.

of the characteristics of  $L$ , but they are not used for further illustration of the results in this paper.

## 5. Discussions

### 5.1. Annual mean $L$ and $S$

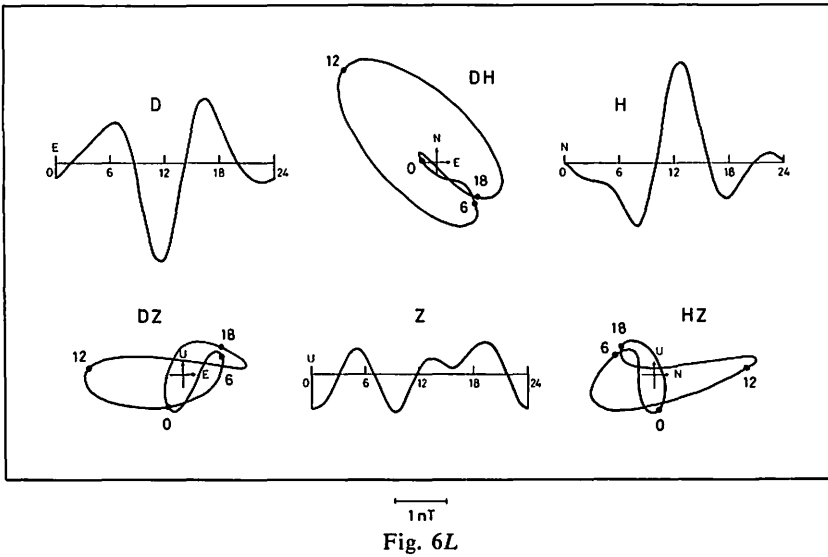


Fig. 6L

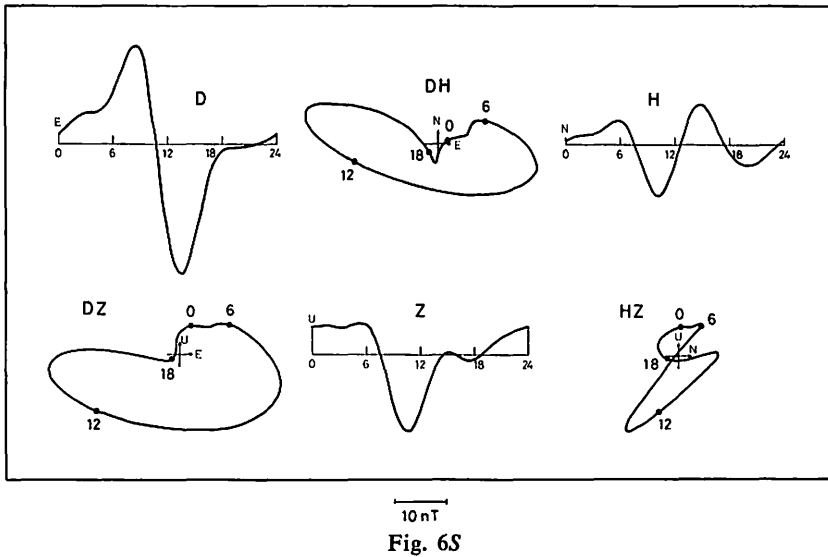


Fig. 6S

Fig. 6(L, S). Daygraphs and vector diagrams for the *L* and *S* variations for the division "all" in Tables 2(L, S). Curves for *L* refer to the epoch of new moon, and are drawn as if during the lunar day centered at new moon the sun and moon remained on the same meridian. The *L* curves are magnified tenfold compared with the *S* curves.

The annual mean *L* determined from the data as a whole is illustrated in Fig. 5L by harmonic dials. In this figure it is clear that the outstanding harmonics are those of  $L_2$ . It indicates that *L* is mainly semidiurnal. This is also well shown in Fig. 6L

Table 7. Ratios of the range for  $S$  to that for  $L$ .

	$D$	$H$	$Z$
all	13.9	5.6	15.5
winter	6.3	2.6	7.0
equinox	13.0	8.3	13.2
summer	10.1	5.0	7.1
low	13.5	5.1	12.3
medium	13.4	5.5	14.4
high	15.3	6.0	18.7
quiet	13.2	6.2	15.6
medium	15.9	5.1	15.8
disturbed	13.9	5.6	15.5

by daygraphs and vector diagrams, with two maxima and two minima per day. However, this characteristic is not so clear for  $Z$ . This is probably due to the oceanic dynamo effect (see section 5.10.).

In contrast to  $L$ ,  $S$  is mainly diurnal. In Fig. 5 $S$  the outstanding harmonics for  $D$  and  $Z$  are those of  $S_1$ , and the variations in Fig. 6 $S$  related to  $D$  and  $Z$  show one maximum and one minimum each day. However, this diurnal characteristic for  $S$  does not hold for  $H$ : the amplitude of  $S_1$  is much smaller than those of the other three harmonics, and the variation is rather semidiurnal. This may be explained by the fact that Kakioka is very close to the focus latitude of the  $S$  current system.

Daygraphs and vector diagrams for both  $L$  and  $S$  show that the daytime variations exceed those at night. This feature for  $L$  is specially well shown by the half-monthly variations of  $L$  in Figs. 3 $L$  and 4 $L$ . The amplitudes of harmonic vectors in Fig. 3 $L$  or the diameters of the ellipses in Fig. 4 $L$  for the daytime are much larger than those around midnight. The reason why this characteristic is not seen for  $L(Z)$  is again to be sought in the oceanic dynamo effect.

The above-mentioned characteristics of  $L$  and  $S$  are generally seen for the results from the other subdivisions of data, especially for the subdivisions which correspond to the annual mean  $L$  and  $S$  variations.

In Figs. 5( $L, S$ ) and 6( $L, S$ ) the force-scale for  $L$  is 10 times larger than that for  $S$ . As the figures for  $L$  and  $S$ , as drawn, are rather similar in size, it follows that  $S$  is about ten times as large as  $L$ . However, when the ratio of  $S$  to  $L$  is examined in detail, it shows remarkable differences between elements and seasons. Table 7 gives the ratios of  $S$  to  $L$  calculated from their ranges of daygraphs, for all cases in Tables 2( $L, S$ ). The maximum value is for  $Z$  in the division of high sunspot numbers, and the minimum one is for  $H$  in winter. Each ratio in this table reflects the various features of the  $L$  and  $S$  variations described in the following. And this variability indicates the difficulty of comparing the general intensity of  $L$  with that

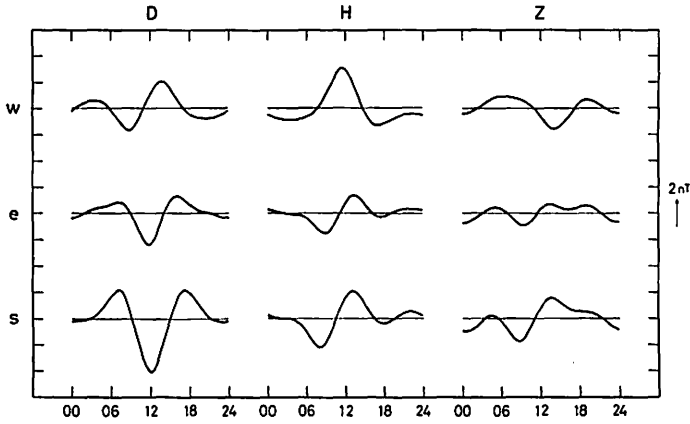


Fig. 7L

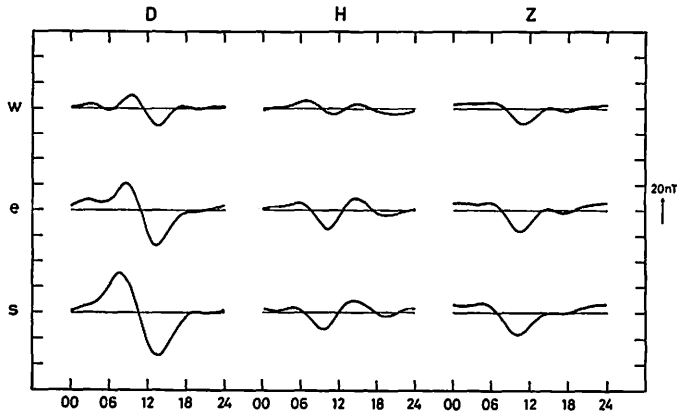


Fig. 7S

Fig. 7(L, S). Daygraphs for the  $L$  and  $S$  variations for three seasonal divisions: winter ( $w$ ), equinox ( $e$ ) and summer ( $s$ ). Curves for  $L$  refer to the epoch of new moon.

of  $S$ .

### 5.2. Seasonal mean $L$ and $S$

The results for the seasonal mean  $L$  and  $S$  are illustrated in Figs. 7(L, S), 8 and 9(L, S). Daygraphs in Fig. 7L indicate that the range and shape of  $L$  variation change remarkably with seasons. The first remarkable point is that the range of each element for equinox is the smallest among the seasons. And for  $D$  and  $Z$ , the ranges for summer are greater than those for winter, and for  $H$  the reverse. Another peculiarity seen from daygraphs is that the shape of variation shows a remarkable difference between winter and summer, and the shape for equinox is rather close to that for summer: those are true for all elements. The epoch of maximum or

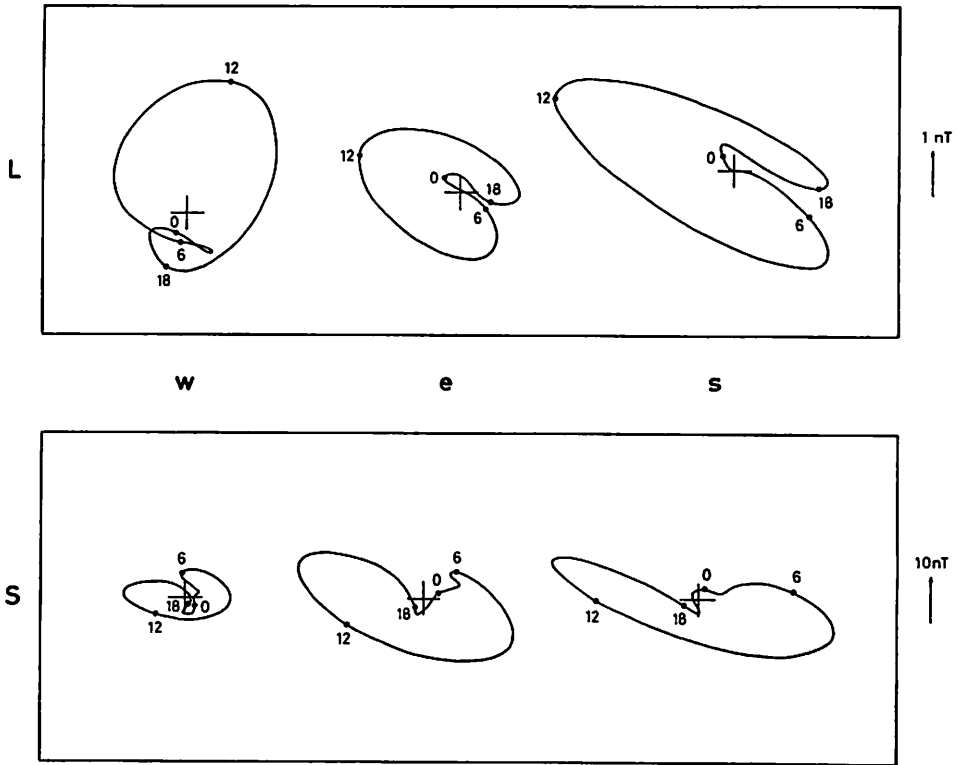


Fig. 8. Horizontal vector diagrams for the *L* and *S* variations for three seasonal divisions: winter (*w*), equinox (*e*) and summer (*s*). The diagrams for *L* refer to the epoch of new moon.

minimum changes from winter to summer by about  $-4$  hours for *D*,  $-2$  hours for *H* and  $+6$  hours for *Z*.

On the other hand, it is clear from Fig. 7*S* that the shape of *S* variations changes little with seasons. And their ranges show the minimum in winter for all elements and they show the maximum in summer for *D* and *Z* and at equinox for *H*. These features for *S* are very different from those for *L*. In the light of our present knowledge, the anomalous features of the seasonal change of *L* at Kakioka are responsible for this difference.

The above-stated features for *L* and *S* from daygraphs are still more clearly indicated by vector diagrams in Fig. 8. The magnitude of the vector diagram, which may be measured by the area of diagram, changes again remarkably with seasons in different ways for *L* and *S*. The change of the shape is also remarkable for *L* and the elongated direction of the diagram is different by about  $90$  degrees between winter and summer. In addition, it is seen that the daytime rotation of the vector diagram is clockwise for both *L* and *S* for all seasons.

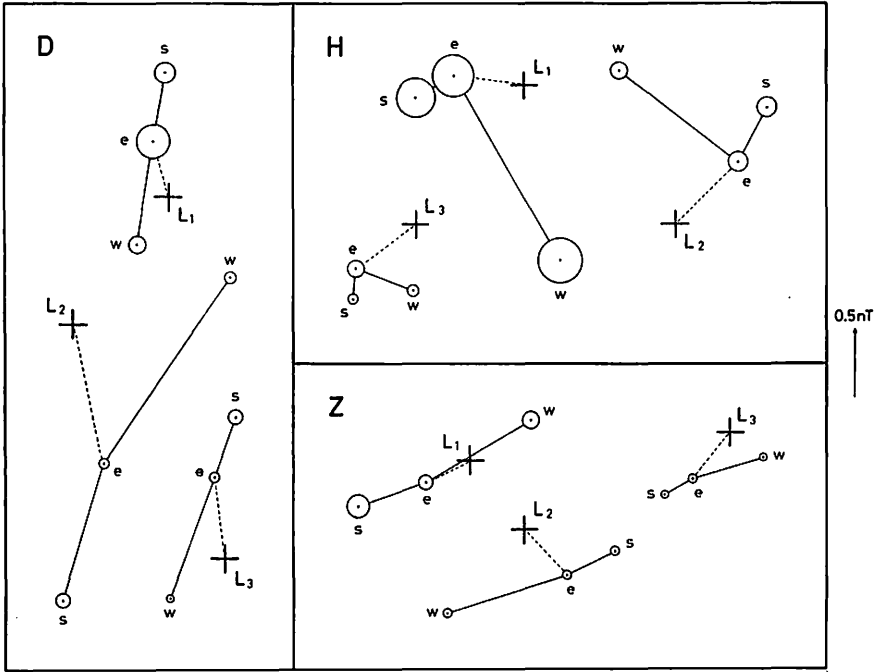


Fig. 9L

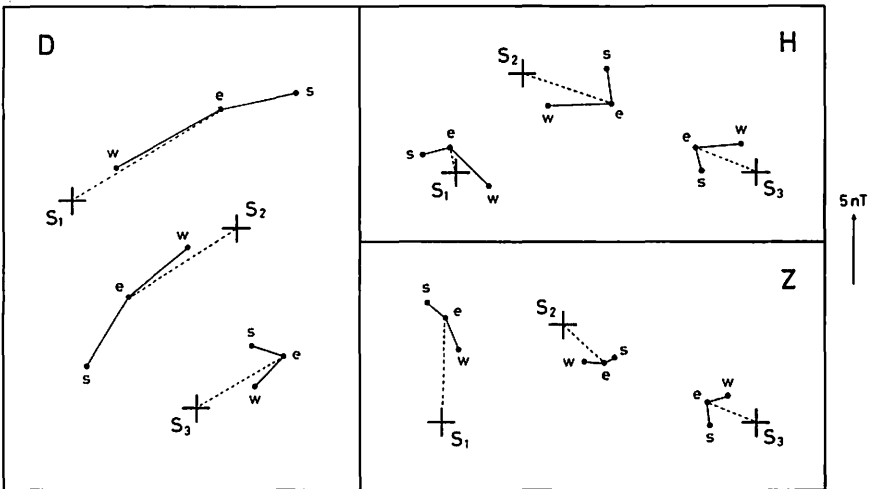


Fig. 9S

Fig. 9(L, S). Harmonic dials for the  $L$  and  $S$  variations for three seasonal divisions: winter ( $w$ ), equinox ( $e$ ) and summer ( $s$ ). The dial vector is drawn only for equinox and those for winter and summer are indicated only by their end points. Numerical suffix indicates the order of the harmonics. For the  $L$  harmonics the vector probable error circles are drawn at the end points of vectors.

In Figs. 9(L, S) the amplitude of each harmonic vector does not necessarily show the same features of the seasonal change as the range of daygraph. This case is found in  $L_3$  and  $L_4$  of all elements,  $L_2$  of Z,  $S_3$  and  $S_4$  of D and Z and  $S_1$  of H. Moreover, the outstanding vector is not necessarily the same as that for the annual mean: this case is found in  $L(H)$  and  $S(D)$  for winter and  $L(Z)$  for summer. As regards the phase of vectors, the change of phase from winter to summer is clockwise for all L vectors except  $L_2(Z)$ , and is anticlockwise for all S vectors except  $S_1(D)$ . And the amount of phase change generally decreases for L and increases for S with increasing harmonics.

As described in section 4, each seasonal division has further been subdivided into six groups according to the sunspot number and magnetic activity in order to examine the changes of L and S with these parameters. Here, the results are looked at from the viewpoint of the seasonal change. In Figs. 15L and 20L, it is clear that the seasonal changes of L for the six subdivisions according to the sunspot number and magnetic activity are very similar to that shown in Fig. 8, though the changes of

Table 8L. Ratios of the seasonal range to the annual mean range for L.

		winter/annual	equinox/annual	summer/annual	
all	}	D	1.16±0.03	1.22±0.04	2.10±0.05
		H	1.51±0.06	0.92±0.05	1.31±0.06
		Z	1.63±0.06	1.31±0.05	2.13±0.08
		D+H	1.23±0.03	1.10±0.03	1.78±0.04
		D+H+Z	1.30±0.02	1.16±0.03	1.84±0.03
low	}	D+H	1.01±0.04	1.14±0.05	1.74±0.05
medium		D+H	1.32±0.04	1.14±0.06	1.72±0.06
high		D+H	1.31±0.05	1.08±0.06	1.86±0.07
quiet	}	D+H	1.01±0.05	0.97±0.05	1.38±0.06
medium		D+H	1.18±0.04	0.94±0.04	1.63±0.05
disturbed		D+H	1.44±0.07	1.18±0.07	1.75±0.08

Table 8S. Ratios of the seasonal range to the annual mean range for S.

		winter/annual	equinox/annual	summer/annual	
all	}	D	0.54	1.12	1.47
		H	0.64	1.41	1.26
		Z	0.85	1.11	1.18
		D+H	0.59	1.27	1.37
		D+H+Z	0.68	1.21	1.30
low	}	D+H	0.61	1.27	1.38
medium		D+H	0.59	1.26	1.39
high		D+H	0.64	1.27	1.33
quiet	}	D+H	0.58	1.27	1.30
medium		D+H	0.58	1.24	1.33
disturbed		D+H	0.76	1.29	1.43

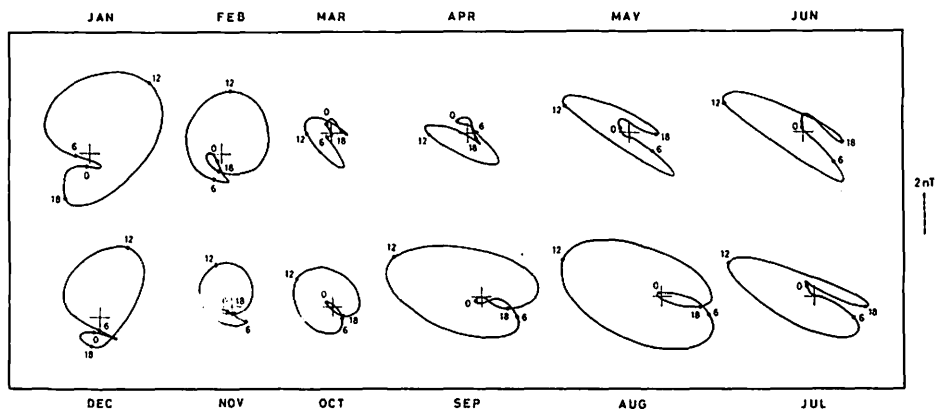


Fig. 10L

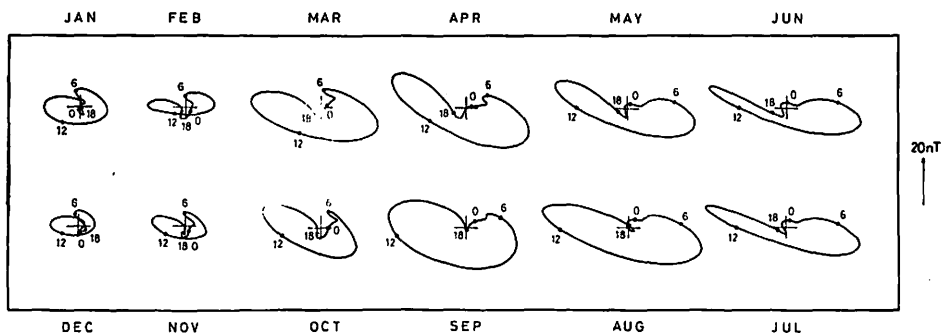


Fig. 10S

Fig. 10(L, S). Horizontal vector diagrams for the  $L$  and  $S$  variations for twelve calendar months.

the magnitude and shape of diagrams between the seasons are somewhat different between subdivisions. The same statement is true for the seasonal change of  $S$ , in comparison of Fig. 8 with Figs. 15S and 20S.

In addition, it is also clear from these figures that, for both  $L$  and  $S$ , the seasonal change is much more pronounced than the changes with the sunspot number and magnetic activity. This is more remarkable for  $L$  than for  $S$ . This fact is very clearly seen by harmonic dials in Figs. 16(L, S) and 21(L, S).

### 5.3. Numerical expression of the seasonal change

The seasonal change of the range of daygraph or the magnitude of vector diagram is examined here by the numerical expression. The range for  $S$  is measured from the daygraph of each element. On the other hand, the range for  $L$  is calculated by the following equation:

$$\text{Range for } L = 2 \sum l_n \quad (9)$$

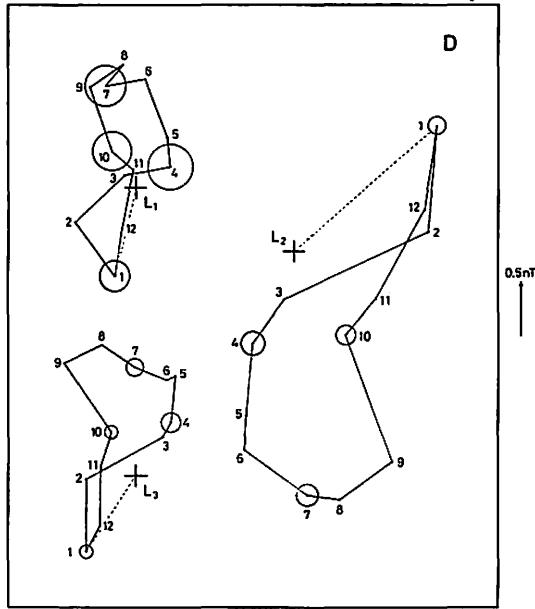


Fig. 11L(a)

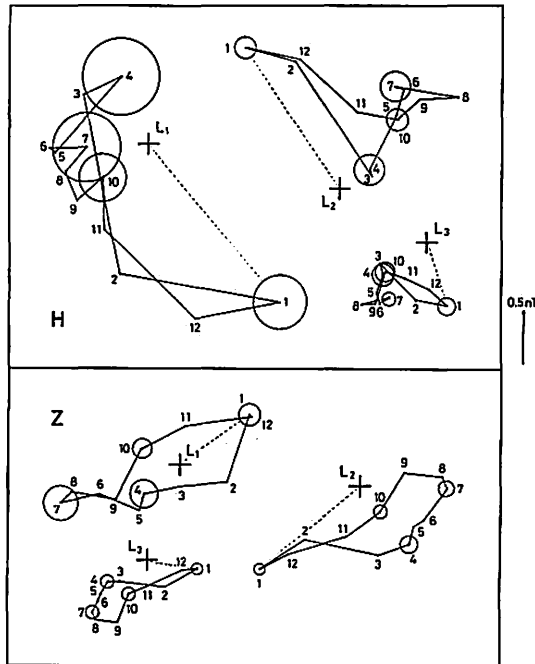


Fig. 11L(b)

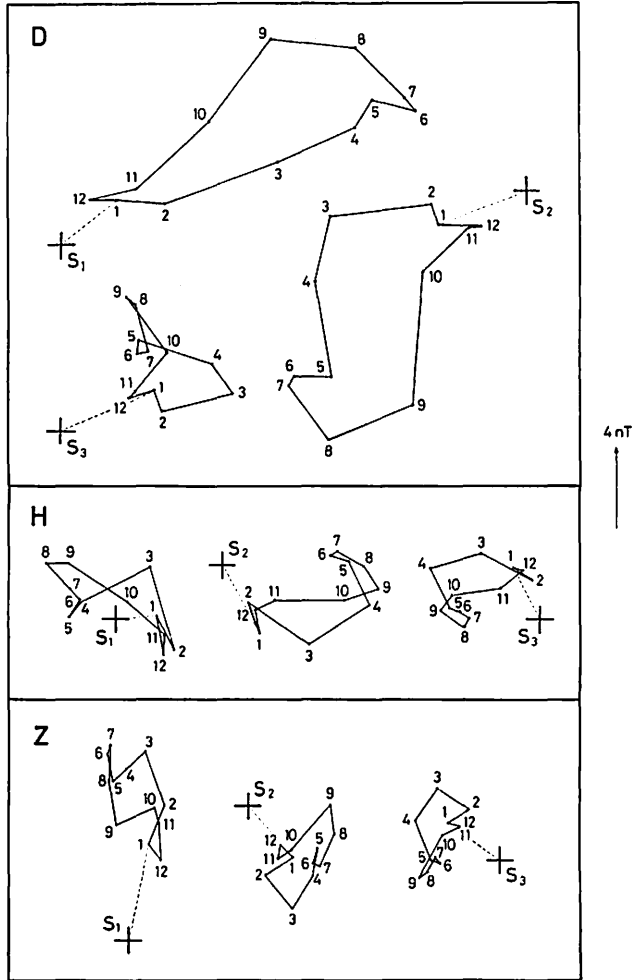


Fig. 11S

Fig. 11(L, S). Harmonic dials for the  $L$  and  $S$  variations for twelve calendar months. The calendar months are denoted by numbers from 1 (January) to 12 (December). The dial vector is drawn only for January and those for the other months are indicated by their end points. For the  $L$  harmonics the vector probable error circles are given at the vector's end points only for a typical month in each season. Harmonic dials for  $L(D)$  are drawn in Fig. 11L (a) and those for  $L(H, Z)$  in Fig. 11L (b).

This nearly represents the range from the daygraph for one half lunation, which is shown in Fig. 2L for the annual mean case, as an example.

For the numerical expression of seasonal change, the ratio of the range for a season to that for the annual mean is calculated for both  $L$  and  $S$ , and it is given

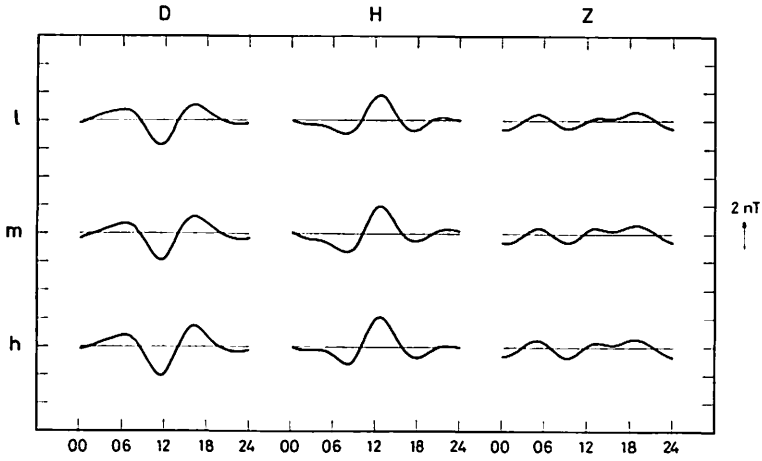


Fig. 12L

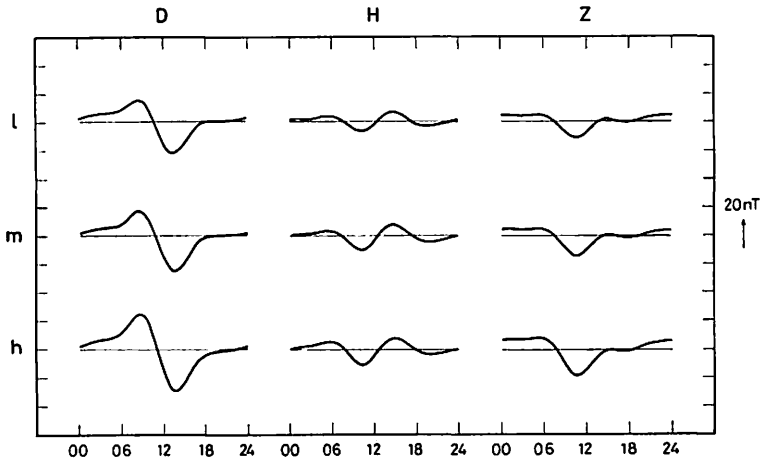


Fig. 12S

Fig. 12(L, S). Daygraphs for the  $L$  and  $S$  variations for three divisions according to sunspot number: low ( $l$ ), medium ( $m$ ) and high ( $h$ ) sunspot numbers.

in Tables 8(L, S) for each of the three elements. Ratios for  $L$  are determined less accurately than those for  $S$ , so the probable errors are given in Table 8L. And the mean values of  $D$  and  $H$  (the heading  $D+H$ ) and of the three elements (the heading  $D+H+Z$ ) are also included. Mean values relating to  $L$  are weighted means, with the weight of the inverse of the square of each probable error. The value of  $D+H$  nearly corresponds to the result estimated with the eye from the magnitude of the horizontal vector diagram. As  $L(Z)$  includes a fairly large part due to the oceanic dynamo effect (see section 5.10.), the value of  $D+H$  for  $L$  may be less affected by the oceanic dynamo

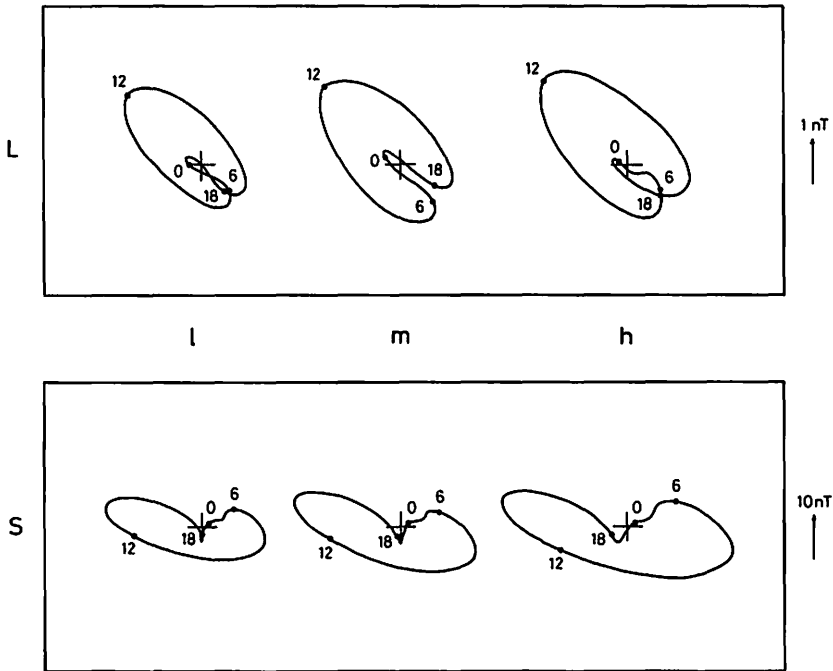


Fig. 13. Horizontal vector diagrams for the  $L$  and  $S$  variations for three divisions according to sunspot number: low ( $l$ ), medium ( $m$ ) and high ( $h$ ) sunspot numbers.

than the value of  $D+H+Z$ .

Comparing the values between  $L$  and  $S$ , remarkable differences are clearly seen. The main difference is in the ratio for winter. The ratio of  $L$  for winter is much greater than unity and is about twice as large as that of  $S$ .

In addition, Tables 8( $L, S$ ) give the seasonal ratios for the six subdivisions according to the sunspot number and magnetic activity, but only the mean of  $D+H$ . It is clear for both  $L$  and  $S$  that the seasonal changes for these six subdivisions are nearly similar to each other, though the values of the ratio are somewhat different between subdivisions.

#### 5.4. Monthly mean $L$ and $S$

The seasonal changes of  $L$  and  $S$  are understood more precisely from the results of the monthly analysis, which are illustrated in Figs. 10( $L, S$ ) and 11( $L, S$ ). Fig. 10L shows the remarkable changes of the magnitude and shape of the vector diagram for  $L$  throughout the year. As to the magnitude, its change is roughly semiannual. The maximum occurs in the winter and summer months and the minimum in the equinoctial months. On the other hand, the shape seems to show nearly annual

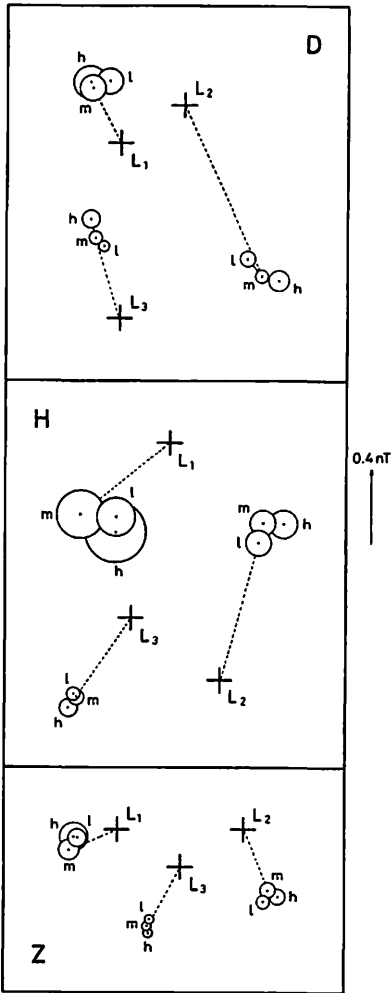


Fig. 14L

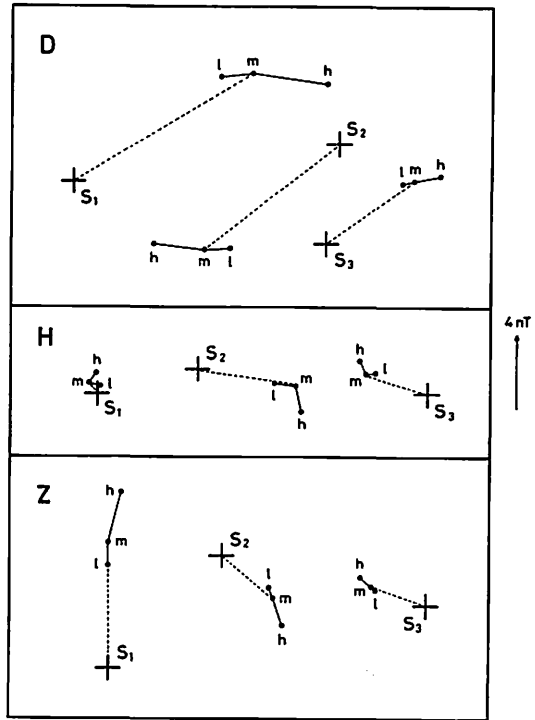


Fig. 14S

Fig. 14(L, S). Harmonic dials for the  $L$  and  $S$  variations for three divisions according to sunspot number: low ( $l$ ), medium ( $m$ ) and high ( $h$ ) sunspot numbers. The dial vector is drawn only for the division  $m$  and those for the other divisions are indicated by their end points.

change: roughly speaking, the shape may be classified into the winter type and the summer one. Change of type from winter to summer occurs suddenly around the end of February, and that from summer to winter occurs gradually from November to December. The months in which the shape changes correspond to the months in which the minimum magnitude occurs. In addition, it seems that September and November should be included in the summer and the equinoctial season, respectively,

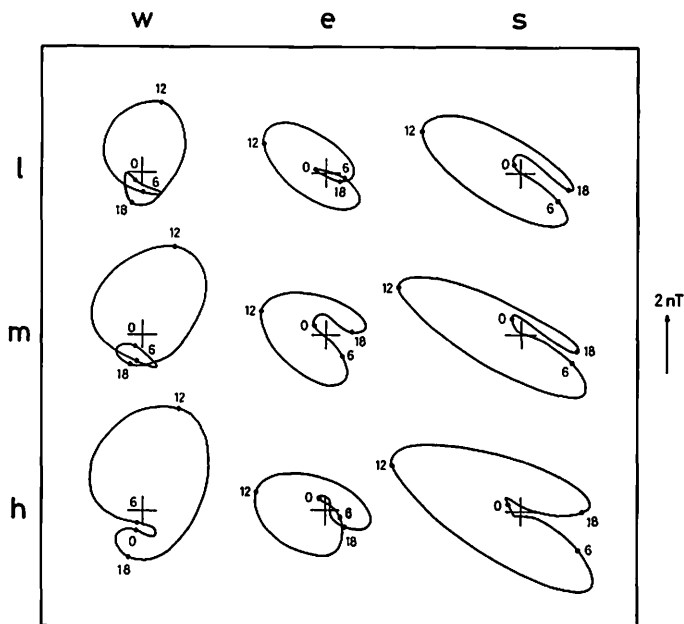


Fig. 15L

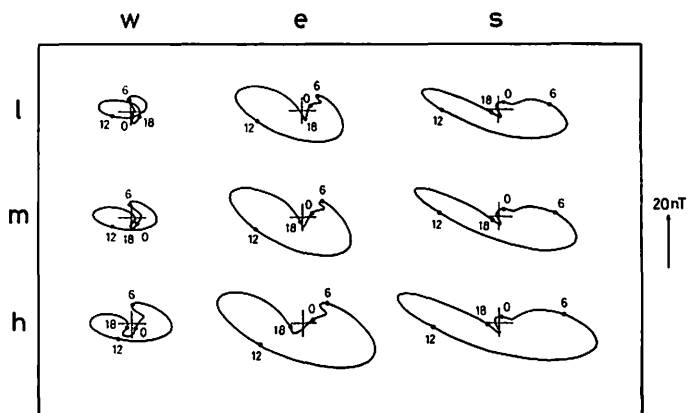


Fig. 15S

Fig. 15(L,S). Horizontal vector diagrams for the  $L$  and  $S$  variations for nine groups divided by three seasonal divisions ( $w, e, s$ ) and three divisions according to sunspot number ( $l, m, h$ ).

if both magnitude and shape are taken into consideration. As is clear from this fact, the annual change of magnitude and shape is, of course, not symmetrical.

Fig. 10S also shows the changes of the magnitude and shape of vector diagrams for  $S$  throughout the year. The change of magnitude is roughly annual: a minimum

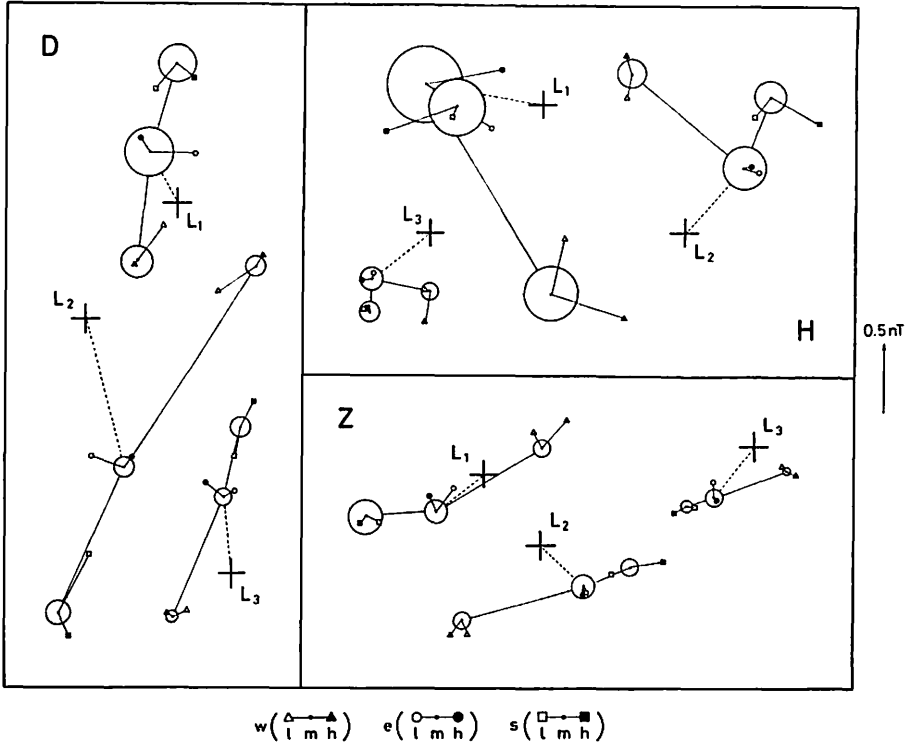


Fig. 16L

in the winter months and a maximum in the summer months. The change of shape is not so remarkable as that for  $L$ .

Figs. 11(L, S) show similar features to those noted for Figs. 10(L, S). These figures add much information on the phase, especially the remarkable difference of the months of December, January and February from the remaining nine months for  $L$ , and the difference between the spring months (March and April) and the autumn months (September and October) for both  $L$  and  $S$ .

5.5. Changes of  $L$  and  $S$  with sunspot number

Figs. 12(L, S) and 13 show the changes of  $L$  and  $S$  with the sunspot number by daygraphs and vector diagrams, respectively. All daygraphs and vector diagrams in these figures correspond to the annual mean and show an increase of the range or magnitude with the increasing sunspot number, with little apparent change of shape.

Figs. 14(L, S) illustrate the harmonic vectors for the divisions of the sunspot number. For  $S$ , each amplitude of all harmonic vectors for all elements increases with the increasing sunspot number, and each phase of all harmonic vectors for  $D$  and  $Z$  changes clockwise with the increasing sunspot number. The change for  $H$  is not

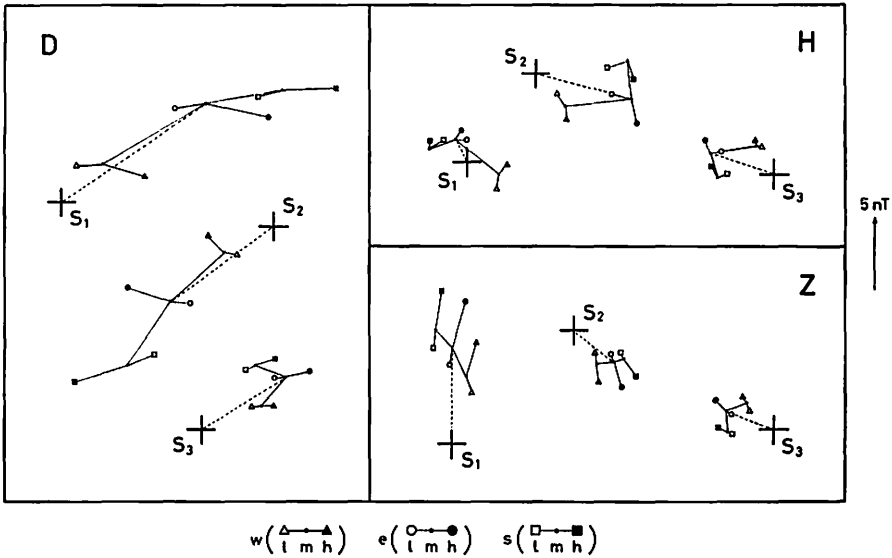


Fig. 16S

Fig. 16(L, S). Harmonic dials for the *L* and *S* variations for nine groups divided by three seasonal divisions (*w, e, s*) and three divisions according to sunspot number (*l, m, h*). The dial vector is drawn only for the group (*e, m*) and those for the other groups are indicated by their end points. For the *L* harmonics the probable error circles are drawn at the end points of vectors only for the groups related to the division *m*.

Table 9L. Values of  $10^4m$  for the range of *L*.

	<i>D</i>	<i>H</i>	<i>Z</i>	<i>D+H</i>	<i>D+H+Z</i>
all	$18 \pm 3$	$18 \pm 10$	$9 \pm 4$	$18 \pm 3$	$15 \pm 2$
winter	$50 \pm 18$	$53 \pm 23$	$32 \pm 7$	$51 \pm 14$	$36 \pm 6$
equinox	$16 \pm 13$	$3 \pm 40$	$20 \pm 10$	$15 \pm 12$	$18 \pm 8$
summer	$27 \pm 14$	$38 \pm 19$	$26 \pm 6$	$31 \pm 11$	$27 \pm 5$
quiet	$-11 \pm 19$	$-23 \pm 18$	$-28 \pm 23$	$-17 \pm 13$	$-20 \pm 11$
medium	$26 \pm 13$	$4 \pm 16$	$34 \pm 9$	$17 \pm 10$	$27 \pm 7$
disturbed	$21 \pm 28$	$63 \pm 61$	$7 \pm 9$	$28 \pm 25$	$9 \pm 8$

Table 9S. Values of  $10^4m$  for the range of *S*.

	<i>D</i>	<i>H</i>	<i>Z</i>	<i>D+H</i>	<i>D+H+Z</i>
all	47	42	72	45	54
winter	66	43	70	55	60
equinox	51	41	70	46	54
summer	42	36	54	39	44
quiet	50	34	69	42	51
medium	49	39	71	44	53
disturbed	45	45	65	45	52

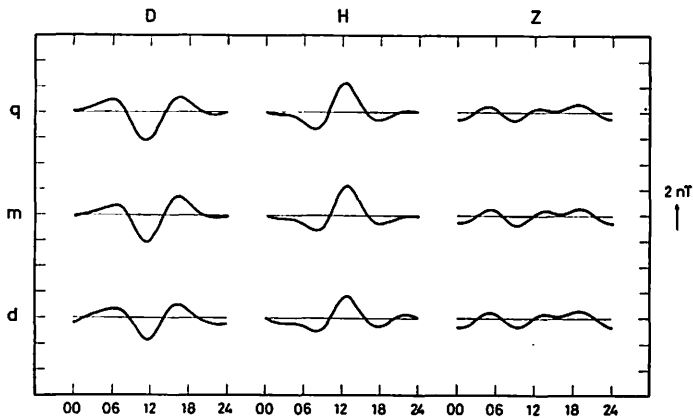


Fig. 17L

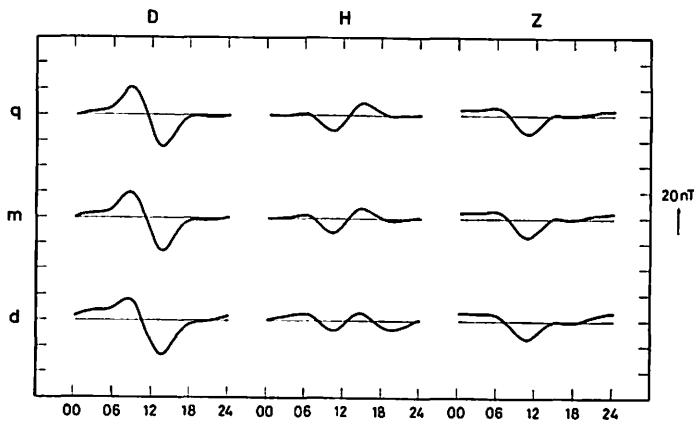


Fig. 17S

Fig. 17(L, S). Daygraphs for the  $L$  and  $S$  variations for three divisions according to magnetic activity: magnetically quiet ( $q$ ), medium ( $m$ ) and disturbed ( $d$ ) days.

systematic but its features are the same for all harmonics. For  $L$ , the amplitude of main vectors generally increases with the increasing sunspot number. This is clear for  $L_2(D, H)$  and  $L_3(D, Z)$ . However, no systematic change is seen for the phase of vectors.

In all Figs. 12(L, S), 13 and 14(L, S), the change of  $L$  with the sunspot number is less pronounced than that of  $S$ . This is examined by the numerical expression of the sunspot cycle change in the next section.

Figs. 15(L, S) and 22(L, S) illustrate by vector diagrams the sunspot cycle changes of  $L$  and  $S$  for the subdivisions according to season and magnetic activity. The characteristics for  $S$  seen in these figures are nearly the same as those mentioned above

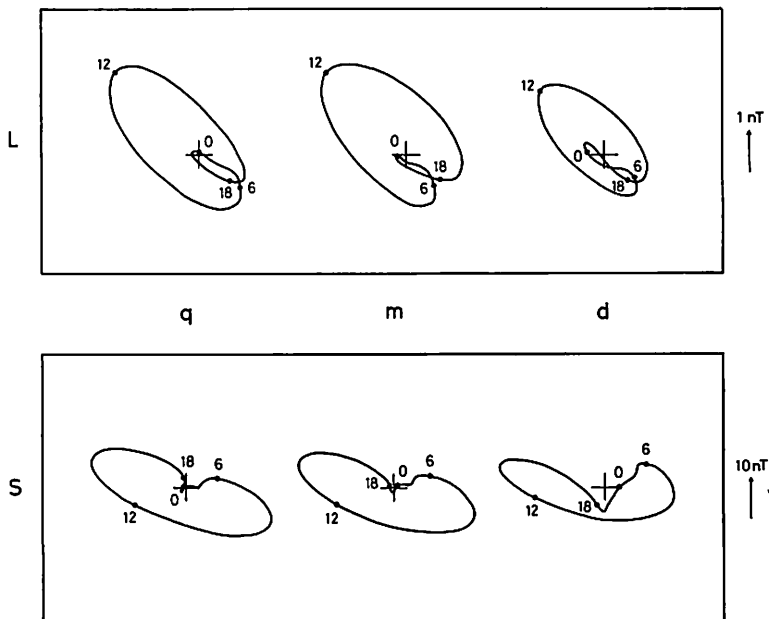


Fig. 18. Horizontal vector diagrams for the  $L$  and  $S$  variations for three divisions according to magnetic activity: magnetically quiet ( $q$ ), medium ( $m$ ) and disturbed ( $d$ ) days.

in regard to Fig. 13: the magnitude increases with the increasing sunspot number though the rate of change is different between subdivisions, and the shape shows little change in all subdivisions except the subdivision of winter. However, the characteristics for  $L$  are not necessarily the same as those noted in regard to Fig. 13. In Figs. 15 $L$  and 22 $L$ , the change of magnitude is different from subdivision to subdivision: increase for the subdivisions of winter, summer and disturbed days, and decrease for those of quiet days. Moreover, the change of shape for  $L$  is somewhat irregular, especially for the subdivisions of quiet days and disturbed days.

Figs. 16( $L, S$ ) and 23( $L, S$ ) illustrate the change of each harmonic vector with the sunspot number for the subdivisions according to season and magnetic activity. The information for  $S$  from these figures is generally similar to that from Fig. 14 $S$ , but the information for  $L$  is much more complex than that from Fig. 14 $L$ .

As noted above, it is clear in Figs. 15( $L, S$ ) and 16( $L, S$ ) that the changes of  $L$  and  $S$  with the sunspot number is less pronounced than their seasonal changes. This fact is more remarkable for  $L$  than for  $S$ .

### 5.6. Numerical expression of the sunspot cycle change

The changes of  $L$  and  $S$  with the sunspot number have generally been studied by Wolf's formula, that is, the linear relationship between the sunspot number  $R$  and the

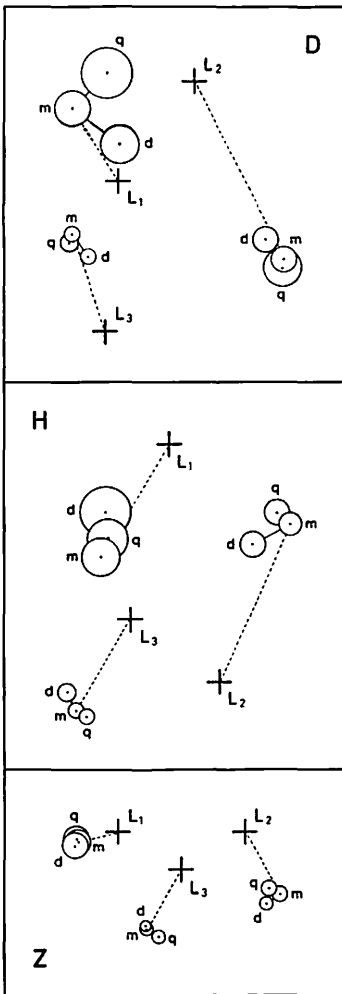


Fig. 19L

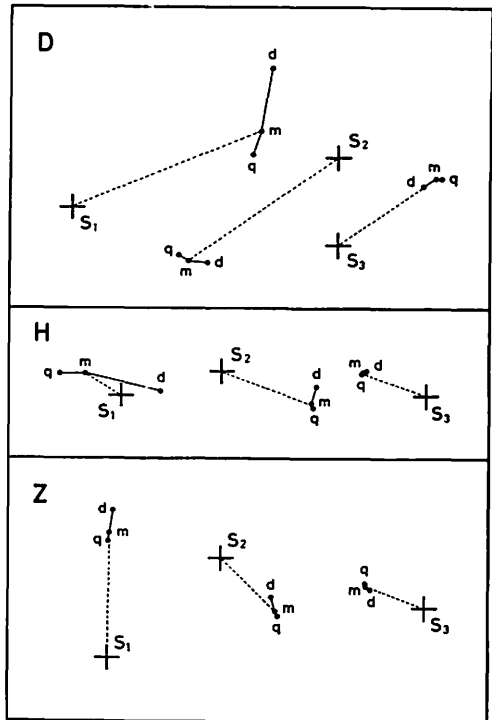


Fig. 19S

Fig. 19(L, S). Harmonic dials for the  $L$  and  $S$  variations for three divisions according to magnetic activity: magnetically quiet ( $q$ ), medium ( $m$ ) and disturbed ( $d$ ) days. The dial vector is drawn only for the division  $m$  and those for the other divisions are indicated by their end points.

range of  $L$  or  $S$ . The relationship is expressed as follows:

$$\text{Range} = A(1 + mR) \tag{10}$$

where  $A$  and  $m$  are constants to be determined from the data. The value of  $10^4 m$  represents the percentage change in the range associated with an increase in  $R$  from 0 to 100 and is a good index of the sunspot cycle change. However, it should be

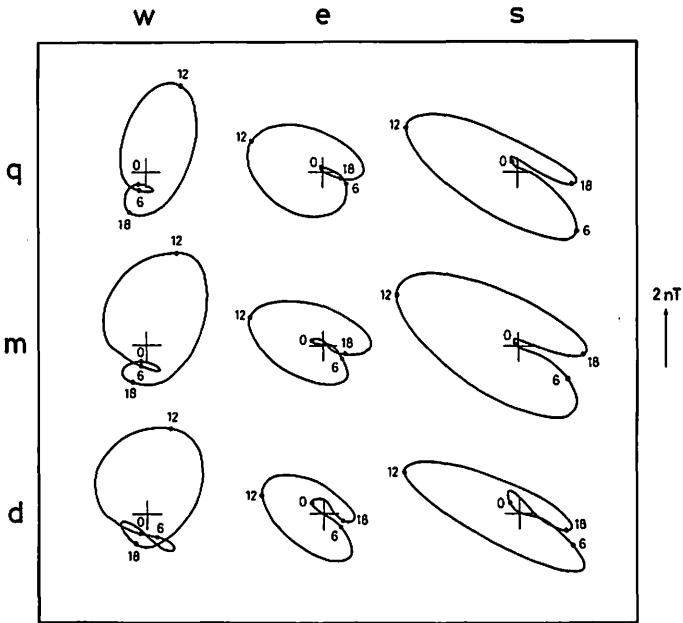


Fig. 20L

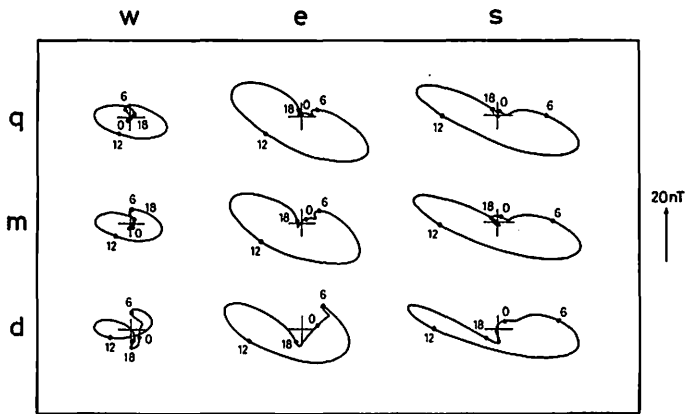


Fig. 20S

Fig. 20(L, S). Horizontal vector diagrams for the  $L$  and  $S$  variations for nine groups divided by three seasonal divisions ( $w, e, s$ ) and three divisions according to magnetic activity ( $q, m, d$ ).

remembered that the change of the shape of  $L$  and  $S$  with the sunspot number is not taken into consideration in the application of this formula. The ranges for  $L$  and  $S$  are those defined in section 5.3. The ranges for each sunspot division are fitted to Eq. (10) by the method of least squares. For  $L$  the calculation of  $m$  was carried out by weighting each range inversely as the square of its probable error. And the probable

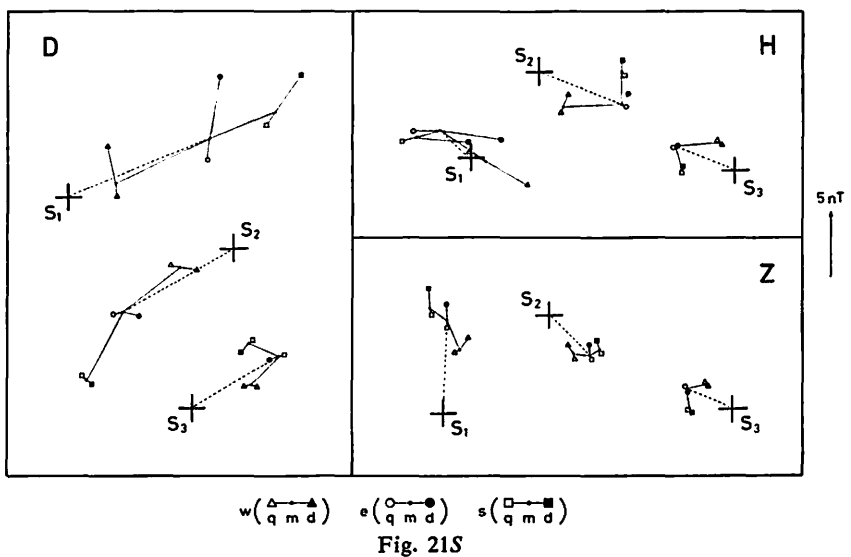
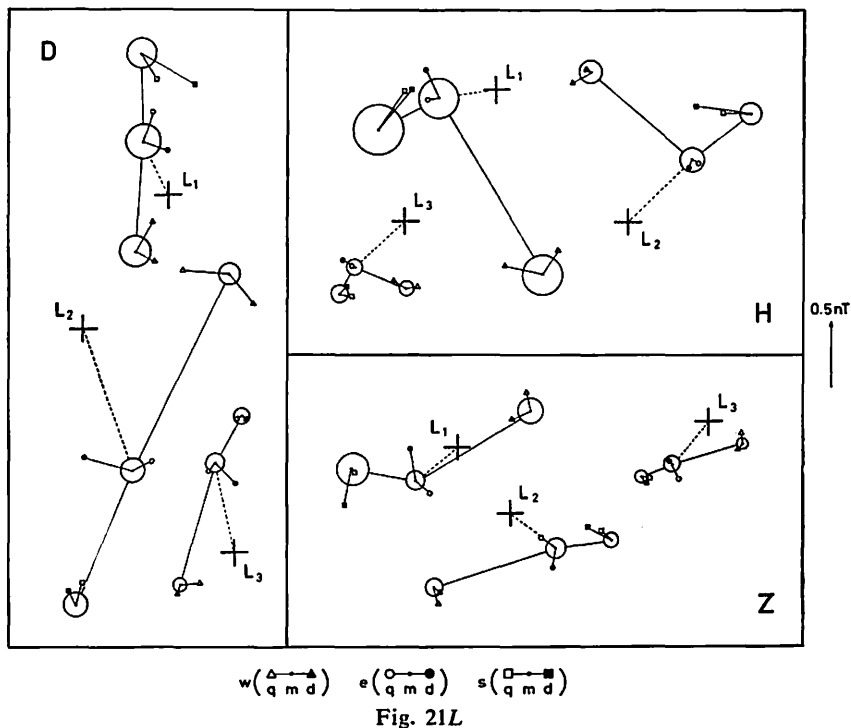


Fig. 21(L, S). Harmonic dials for the L and S variations for nine groups divided by three seasonal divisions (*w, e, s*) and three divisions according to magnetic activity (*q, m, d*). The dial vector is drawn only for the group (*e, m*) and those for the other groups are indicated by their end points. For the L harmonics the probable error circles are drawn at the end points of vectors only for the groups related to the division *m*.

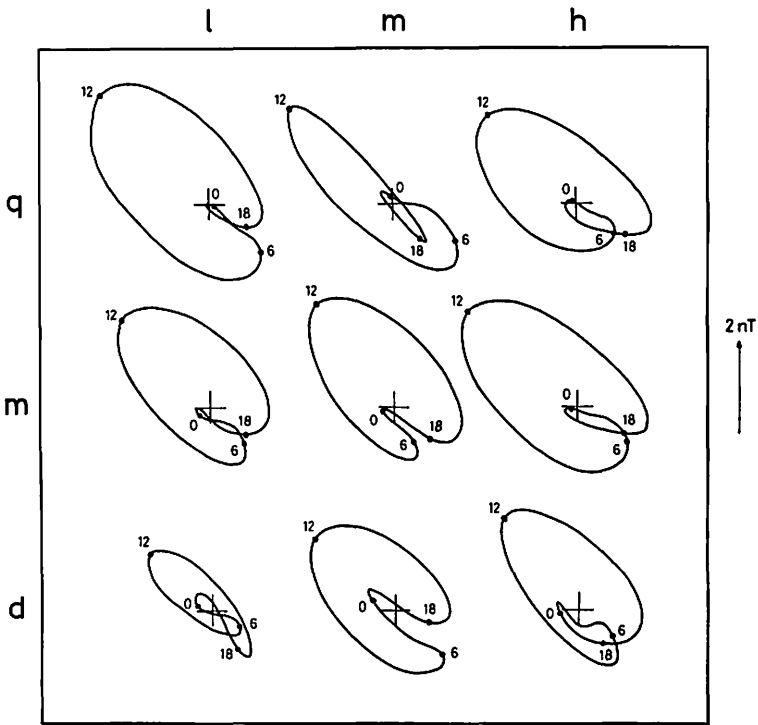


Fig. 22L

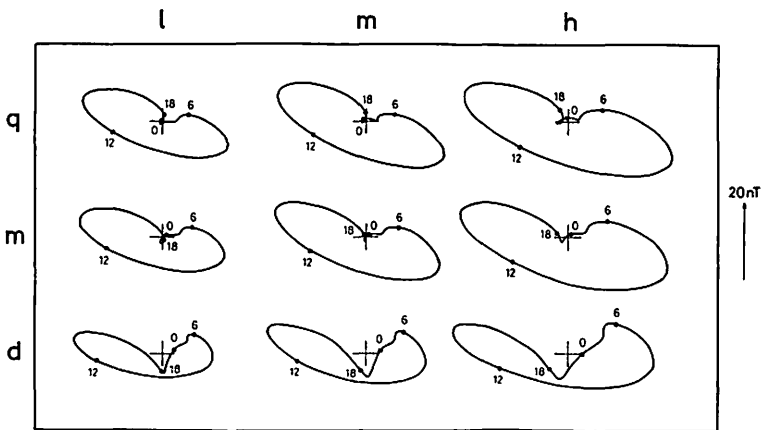


Fig. 22S

Fig. 22(L, S). Horizontal vector diagrams for the *L* and *S* variations for nine groups divided by three divisions according to sunspot number (*l, m, h*) and three divisions according to magnetic activity (*q, m, d*).

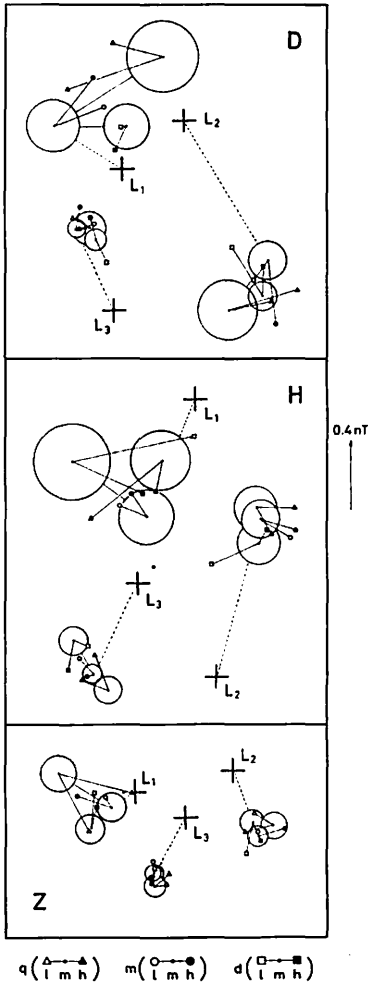


Fig. 23L

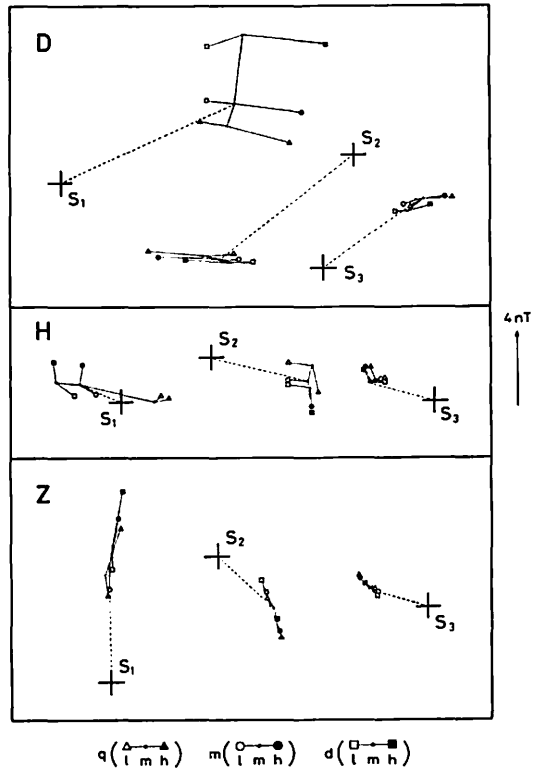


Fig. 23S

Fig. 23(L, S). Harmonic dials for the  $L$  and  $S$  variations for nine groups divided by three divisions according to sunspot number ( $l, m, h$ ) and three divisions according to magnetic activity ( $q, m, d$ ). The dial vector is drawn only for the group ( $m, m$ ) and those for the other groups are indicated by their end points. For the  $L$  harmonics the probable error circles are drawn at the end points of vectors only for the groups related to the division  $m$  according to magnetic activity.

Table 10L. Values of  $10^2 m'$  for the range of  $L$ .

	$D$	$H$	$Z$	$D+H$	$D+H+Z$
all	$-27 \pm 6$	$-19 \pm 8$	$3 \pm 4$	$-24 \pm 5$	$-8 \pm 3$
winter	$15 \pm 17$	$-5 \pm 13$	$-11 \pm 6$	$2 \pm 10$	$-8 \pm 5$
equinox	$-21 \pm 12$	$-2 \pm 23$	$7 \pm 9$	$-17 \pm 11$	$-3 \pm 7$
summer	$-3 \pm 9$	$-13 \pm 25$	$-1 \pm 7$	$-4 \pm 8$	$-2 \pm 5$
low	$-41 \pm 11$	$-48 \pm 11$	$0 \pm 12$	$-45 \pm 8$	$-31 \pm 7$
medium	$-17 \pm 13$	$-1 \pm 20$	$-16 \pm 15$	$-12 \pm 11$	$-14 \pm 9$
high	$-28 \pm 23$	$8 \pm 27$	$20 \pm 30$	$-13 \pm 18$	$-5 \pm 15$

Table 10S. Values of  $10^2 m'$  for the range of  $S$ .

	$D$	$H$	$Z$	$D+H$	$D+H+Z$
all	-4	-33	2	-19	-11
winter	-19	22	-3	2	0
equinox	-7	-29	4	-18	-11
summer	5	-26	3	-11	-6
low	-1	-34	3	-18	-11
medium	-3	-30	5	-17	-9
high	-4	-31	1	-18	-11

error of  $m$  was deduced in considering both the probable errors of the range used in the determination of  $m$  and residuals from the best fitted straight line. The method of determination of  $m$  for  $S$  is similar, except that each range is given unit weight and no probable errors are determined.

Values of  $10^4 m$  for the three elements are given under "all" in Tables 9( $L, S$ ). The mean values of  $D$  and  $H$  and of the three elements are also included. In addition, the values of  $10^4 m$  for each subdivision according to season and magnetic activity are also calculated in the same way and are given for each of the subdivisions.

From the results in Tables 9( $L, S$ ) the following characteristics emerge. The values of  $10^4 m$  show very considerable difference between elements, seasons and subdivisions according to magnetic activity. This is more remarkable for  $L$  than for  $S$ . However, the difference for  $L$  is not necessarily significant, when the probable errors are strictly taken into consideration. In addition, the difference of the values between  $L$  and  $S$  is also clear. The value for  $L$  is generally much less than the corresponding one for  $S$ . For the case of "all", the value of  $D+H$  for  $S$  is about twice as large as that for  $L$ .

### 5.7. Changes of $L$ and $S$ with magnetic activity

Figs. 17( $L, S$ ) and 18 show the changes of  $L$  and  $S$  with magnetic activity by daygraphs and vector diagrams, respectively. All daygraphs and vector diagrams in these figures correspond to the annual mean. Those for  $L$  except the daygraphs

Table 11S. Harmonic components of *SD*. The unit is 0.1 nT for  $s_n$ , degrees for  $\sigma_n$ .

		$s_1$	$\sigma_1$	$s_2$	$\sigma_2$	$s_2$	$\sigma_2$	$s_4$	$\sigma_4$	
Declination <i>D</i>										
all	{	<i>SDm</i>	13	70	6	333	3	176	1	25
		<i>SDd</i>	47	78	16	346	10	202	3	47
		<i>SDa</i>	28	76	10	344	6	197	2	42
winter	{	<i>SDd</i>	38	99	20	350	10	175	3	19
equinox			64	82	19	355	11	198	4	34
summer			47	54	9	317	12	226	3	89
low	{	<i>SDd</i>	39	86	12	338	8	198	3	33
medium			49	81	15	349	11	210	3	61
high			55	69	19	349	13	196	2	46
Horizontal intensity <i>H</i>										
all	{	<i>SDm</i>	13	358	2	103	1	14	1	200
		<i>SDd</i>	55	350	11	81	2	8	2	210
		<i>SDa</i>	32	351	6	82	1	9	1	208
winter	{	<i>SDd</i>	50	331	14	68	3	320	2	188
equinox			67	356	10	80	3	343	3	211
summer			51	360	11	100	4	76	2	236
low	{	<i>SDd</i>	47	359	12	88	2	12	2	203
medium			54	350	12	82	3	18	2	226
high			64	343	11	72	2	354	3	210
Vertical intensity <i>Z</i>										
all	{	<i>SDm</i>	4	84	3	109	1	314	1	178
		<i>SDd</i>	17	82	10	107	4	309	2	183
		<i>SDa</i>	10	82	6	108	2	308	1	182
winter	{	<i>SDd</i>	16	48	11	114	4	302	1	177
equinox			18	91	11	99	4	298	2	164
summer			20	99	10	106	4	331	2	206
low	{	<i>SDd</i>	14	85	9	108	3	300	2	172
medium			17	78	11	111	4	333	2	201
high			20	83	11	102	5	298	1	176

Table 12S. Ratios of the range for *Sq* to that for *SD*.

		<i>D</i>	<i>H</i>	<i>Z</i>	
all	{	<i>Sq/SDm</i>	13.4	8.3	18.7
		<i>Sq/SDd</i>	4.0	1.9	4.8
		<i>Sq/SDa</i>	6.7	3.4	8.2
winter	{	<i>Sq/SDd</i>	2.5	1.1	4.1
equinox			3.4	2.3	5.3
summer			5.9	2.5	5.1
low	{	<i>Sq/SDd</i>	4.0	1.9	4.4
medium			3.8	2.0	4.3
high			4.2	1.9	5.4

of *L(Z)* show a decrease of range or magnitude with increasing magnetic activity, with little apparent change of shape. However, those for *S* show some change of

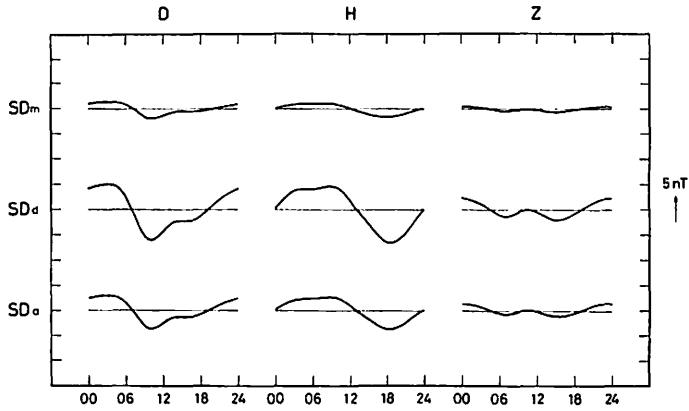


Fig. 24S(a)

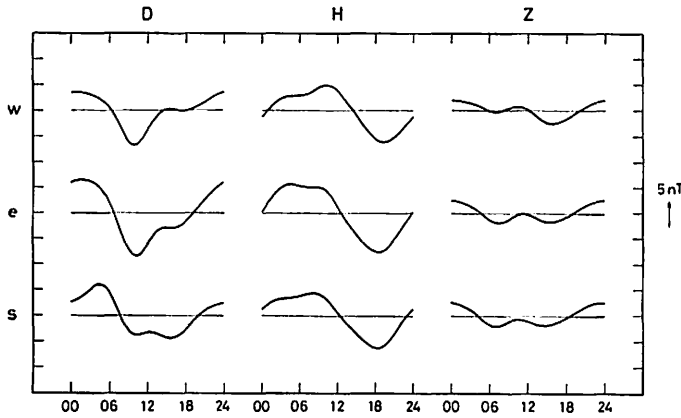


Fig. 24S(b)

shape with magnetic activity. The change of  $S$  with magnetic activity is usually studied in terms of the disturbance daily variation  $SD$  and is examined in section 5.9.

Fig. 19L illustrates the change of  $L$  harmonic vectors with magnetic activity. The change of vectors is not so systematic, but their amplitudes generally decrease with increasing magnetic activity. This is clear for  $L_1(D)$  and  $L_2(D, H)$ .

Figs. 20L and 21L illustrate by vector diagrams and harmonic dials the change of  $L$  with magnetic activity for the subdivisions according to season. Moreover, looking at Figs. 22L and 23L from another angle, we see that they illustrate the change of  $L$  with magnetic activity for the subdivisions according to the sunspot number. In these figures, the change of the magnitude and shape of vector diagrams is small except for the subdivision of low sunspot numbers. And the change of vectors shows the complex difference between subdivisions, elements and harmonics.

#### 5.8. Numerical expression of the change with magnetic activity

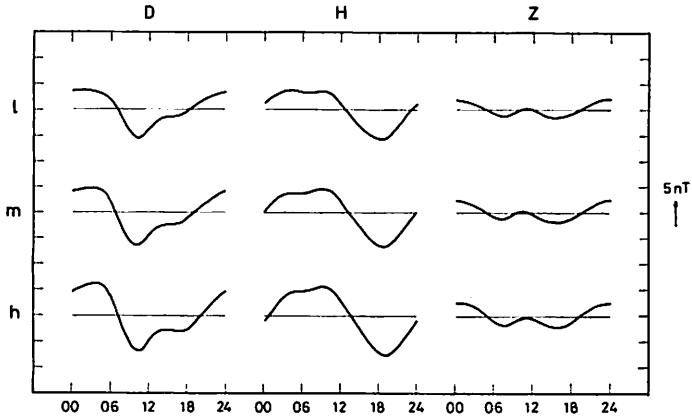


Fig. 24S(c)

Fig. 24S. Daygraphs for the  $SD_m$ ,  $SD_d$  and  $SD_a$  variations for the division "all" in Table 11S (Fig. 24S (a)), for the  $SD_d$  variations for three seasonal divisions ( $w, e, s$ ) (Fig. 24S (b)), and for the  $SD_d$  variations for three divisions according to sunspot number ( $l, m, h$ ) (Fig. 24S (c)).

The changes of  $L$  and  $S$  with magnetic activity are numerically examined here by a formula similar to that of Wolf:

$$\text{Range} = A'(1 + m'C) \tag{11}$$

Here  $C$  denotes the mean value of  $C_i$  index for a division according to magnetic activity. As in the case of the value of  $m$  in section 5.6, the value of  $m'$  is obtained by fitting the ranges for each division to Eq. (11) by the method of least squares.

The values of  $10^2 m'$  are given under "all" in Table 10( $L, S$ ). In addition, the values of  $10^2 m'$  for the subdivisions according to season and sunspot number are also included in the tables. For the calculation of the value of  $m'$ , the change of the shape of daygraphs, which is very remarkable for  $S$ , is not taken into consideration. The results in the tables are very complex and nothing can be said but that the changes of  $L$  and  $S$  generally show a decrease with increasing magnetic activity.

5.9. The disturbance daily variation  $SD$

It is known that  $S$  is composed of two parts, which are the quiet daily variation  $S_q$  and the disturbance daily variation  $SD$ . The  $S$  variation for the division of quiet days  $S(q)$  is taken here to represent  $S_q$ , though it is not necessarily the ideal  $S_q$ , due to some slight disturbance on many of these quiet days. So the  $SD$  variation appears in the  $S$  variation for the division of magnetically medium days  $S(m)$ , disturbed days  $S(d)$  or all days  $S(a)$ . It is convenient to write as follows:

$$SD_m = S(m) - S(q) \tag{12}$$

$$SD_a = S(a) - S(q) \tag{13}$$

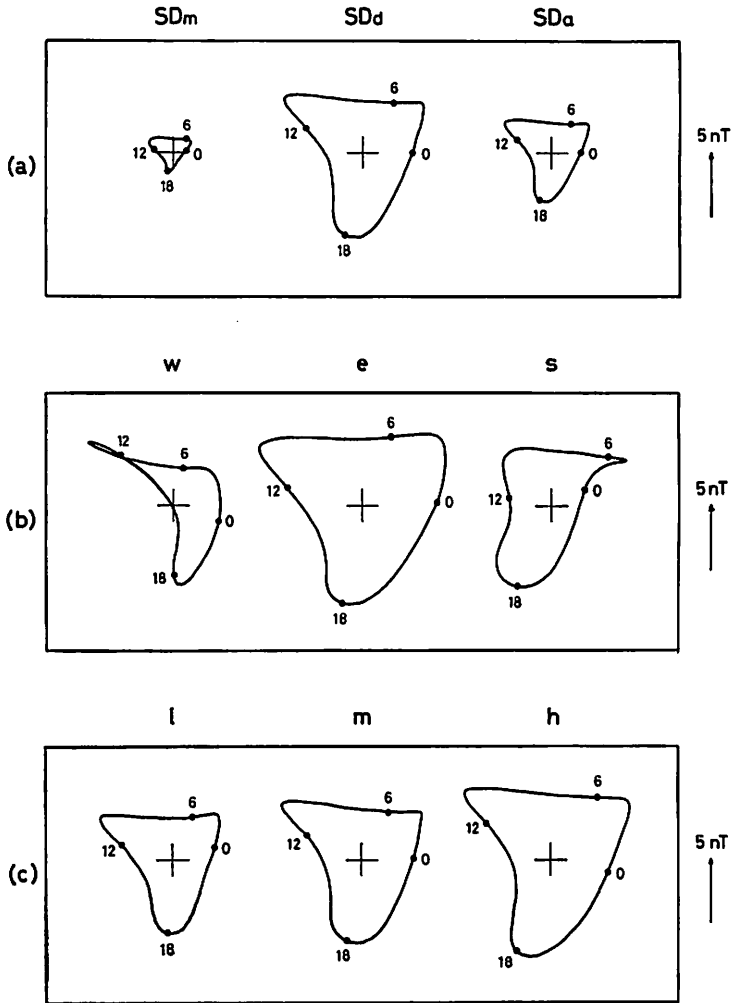


Fig. 25S. Horizontal vector diagrams, (a) for the  $SD_m$ ,  $SD_d$  and  $SD_a$  variations for the division "all" in Table 11S, (b) for the  $SD_d$  variations for three seasonal divisions ( $w$ ,  $e$ ,  $s$ ), and (c) for the  $SD_d$  variations for three divisions according to sunspot number ( $l$ ,  $m$ ,  $h$ ).

$$SD_a = S(a) - S(q) \quad (14)$$

The harmonic coefficients of  $SD_m$ ,  $SD_d$  and  $SD_a$  are computed by the vector subtraction according to the above equations using the results in Tables 2S, 5S and 6S and are given in Table 11S. The  $SD_m$ ,  $SD_d$  and  $SD_a$  given under "all" in this table are obtained from Table 2S and the  $SD_d$  for the subdivisions according to season and sunspot number are obtained from Tables 5S and 6S, respectively. Results in Table 11S are illustrated by daygraphs and vector diagrams in Figs. 24S and 25S, respectively.

Table 13S. Numerical expressions for the features of  $SD$ .

	$D$	$H$	$Z$	$D+H$	$D+H+Z$
(a) Ratios of the range for $SDd$ to that for $SDm$ or $SDa$					
$SDd/SDm$	3.4	4.4	3.9	3.9	3.9
$SDd/SDa$	1.7	1.8	1.7	1.8	1.7
(b) Ratios of the seasonal range to the annual mean range for $SDd$					
winter/annual	0.94	0.98	1.02	0.96	0.98
equinox/annual	1.34	1.18	1.02	1.26	1.18
summer/annual	0.93	0.95	1.08	0.94	0.99
(c) Values of $10^4m$ for the range of $SDd$					
all	41	40	32	41	38

The harmonic dials for  $SD$  are not shown, but the vectors corresponding to  $SD$  are seen in Figs. 19S, 21S and 23S.

In Fig. 19S, it is clear that the outstanding vectors of  $SD$  are those for  $n=1$ , similar to  $Sq$ . But this feature for  $SD$  is much more striking than that for  $Sq$ . Moreover, the direction of the harmonic vectors for  $SD$  is very different from that of the corresponding vector for  $Sq$  except  $S_1(Z)$ . In consequence of these facts, the  $SD$  variation shown in Figs. 24S and 25S is very different from the corresponding  $Sq$  variation shown in Figs. 17S, 18S, 20S and 22S. This fact indicates the different character and origin of the  $Sq$  and  $SD$  parts of  $S$ .

A comparison of the relative magnitude of  $Sq$  and  $SD$  is made in Table 12S by means of the ratio of the corresponding ranges of daygraphs for all the cases in Table 11S. The values of ratio  $Sq/SDd$  are very variable between elements and subdivisions. This again indicates that  $Sq$  and  $SD$  are different phenomena. The overall mean value for  $Sq/SDd$  is 3.9.

In Figs. 24S(a) and 25S(a) the variations of  $SDm$ ,  $SDd$  and  $SDa$  are compared with each other. Clearly, their shapes of variation are very similar, but the relative magnitude of  $SDd$  is about four (two) times as large as that of  $SDm$  ( $SDa$ ). This is the reason why the changes of  $SD$  with season and sunspot number are examined only by the most remarkable  $SDd$ . The values of the ratio  $SDd/SDm$  or  $SDd/SDa$  are given in Table 13S(a).

Figs. 24S(b) and 25S(b) show the seasonal change of  $SDd$ . The outstanding time of the year is the equinox for  $D$  and  $H$ . This is also clear in Table 13S(b), which gives the ratio of the seasonal range to the annual mean one. The seasonal change of the range for  $Z$  is very small. In regard to the seasonal change of the shape of variation, it is clearly seen for  $D$ , but not so for  $H$  and  $Z$ . These features of the seasonal change for  $SDd$  are seen to be very different from those for  $Sq$ , comparing Fig. 25S(b) with Fig. 20S.

Figs. 24S(c) and 25S(c) illustrate the sunspot cycle change of  $SDd$ . These figures

Table 14L. Harmonic components of  $L_I$  and  $L_O$ . The unit is  $0.01 nT$  for  $l_{I,O}$  and  $p.e.$ , degrees for  $\lambda_I$ .

	$l_I$	$p.e.$	$\lambda_I$	$l_O$	$p.e.$	$\lambda_O$
<b>Declination <math>D</math></b>						
all	66	5	288	35	6	310
winter	76	7	47	67	8	341
equinox	69	12	287	35	13	274
summer	178	9	266	23	11	279
low	57	8	280	36	9	314
medium	62	8	290	39	8	303
high	77	10	292	31	12	314
quiet	100	14	280	30	17	358
medium	84	11	295	23	12	304
disturbed	44	11	275	53	13	310
<b>Horizontal intensity <math>H</math></b>						
all	97	8	50	37	9	173
winter	161	17	99	50	18	255
equinox	82	16	9	46	18	137
summer	141	15	23	69	16	154
low	91	11	55	32	13	184
medium	100	14	42	54	15	163
high	102	17	54	26	18	179
quiet	103	12	58	24	13	172
medium	112	11	58	25	13	206
disturbed	92	15	45	48	16	171
<b>Vertical intensity <math>Z</math></b>						
all	47	5	39	69	6	251
winter	68	7	197	41	8	281
equinox	60	6	40	73	7	258
summer	143	9	29	103	10	235
low	42	5	40	69	6	252
medium	50	7	39	69	8	248
high	48	8	39	69	9	254
quiet	45	8	41	63	9	251
medium	43	8	37	62	9	256
disturbed	48	7	41	74	8	251

show that the range of magnitude of  $SDd$  increases with increasing the sunspot number, with little apparent change of shape. This fact is similar to that for  $Sq$ . The numerical expression of the sunspot cycle change of  $SDd$  is given in Table 13S(c) by Wolf's ratio  $m$  in Eq. (10). The values of  $10^4 m$  for  $SDd$  are somewhat different from the corresponding values for  $Sq$  given in Table 9S.

#### 5.10. The oceanic dynamo effect on $L$

The principal mechanism for the production of  $L$  variation is considered to be an ionospheric dynamo. However, the oceanic dynamo is also a fairly large source

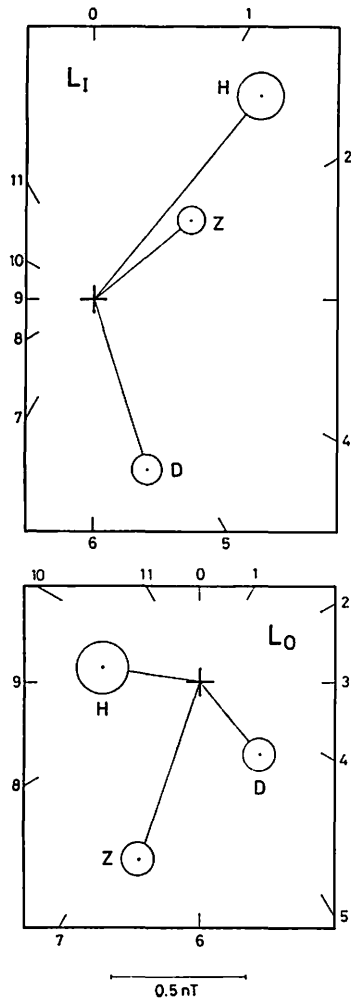


Fig. 26L. Harmonic dials for the  $L_1$  and  $L_0$  variations for the division "all" in Table 14L.

of  $L$ . The oceanic dynamo generates electric currents by the tidal movements of the seas across the lines of force of the Earth's main magnetic field. As the conductivity of the ocean does not exhibit appreciable time variation, the geomagnetic variation resulting from the oceanic dynamo may contribute to  $L_2$  harmonic only. On some assumptions, Malin (1970) showed a method by which the observed  $L_2$  variation can be separated into parts of ionospheric ( $L_1$ ) and oceanic ( $L_0$ ) origin, where  $L_1$  and  $L_0$  are written by the harmonic coefficients as follows:

$$L_1 = l_1 \sin(2\tau + \lambda_1) \tag{15}$$

$$L_0 = l_0 \sin(2\tau + \lambda_0) \tag{16}$$

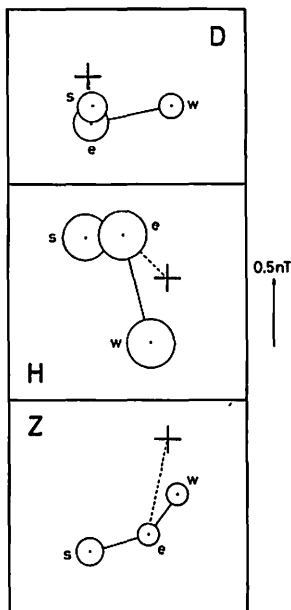


Fig. 27L. Harmonic dials for the  $L_0$  variation for three seasonal divisions ( $w$ ,  $e$ ,  $s$ ). The dial vector is drawn only for the division  $e$  and those for the other divisions are indicated by their end points.

Here we apply his method to the present results of  $L$ . The separated results of  $L_I$  and  $L_O$  are given in Table 14L, only for the cases corresponding to Table 2L, and they are illustrated in Figs. 26L, 27L and 28L by harmonic dials. In Table 14L all  $L_I$  harmonic vectors and all but 5 of 30  $L_O$  vectors are significant. Insignificant harmonic vectors for  $L_O$  are those for  $D$  and  $H$ .

Fig. 26L illustrates the annual mean  $L_I$  and  $L_O$  determined from the results under "all" in Table 2L. In this figure the amplitudes of  $L_I$  for  $D$  and  $H$  are much larger than those of the corresponding  $L_O$ . But, for  $Z$ , the former is less than the latter, and, moreover, the directions of  $L_I$  and  $L_O$  harmonic vectors are nearly opposite to each other. So the oceanic dynamo effect in the observed  $L$  is very remarkable for  $Z$ . This fact explains the different characteristics between  $L(Z)$  and  $L(D, H)$  noted in section 5.1.

The seasonal change of  $L_O$  is illustrated in Fig. 27L and the changes of  $L_O$  with sunspot number and magnetic activity in Fig. 28L. These figures show that  $L_O$  fairly differs between these parameters. For the seasonal divisions,  $L_O$  for winter is remarkably different from that for summer, and for the divisions for sunspot number and magnetic activity some vectors are very different from the overall mean

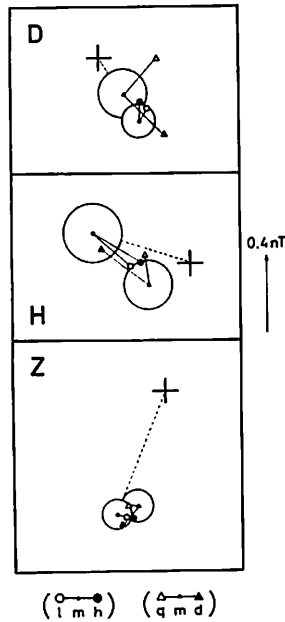


Fig. 28L. Harmonic dials for the  $L_O$  variation for three divisions according to sunspot number ( $l, m, h$ ) and three divisions according to magnetic activity ( $q, m, d$ ). The dial vector is drawn only for the division  $m$  according to sunspot number and those for the other divisions are indicated by their end points. The probable error circles are drawn at the end points of vectors only for the division  $m$  according to sunspot number and the division  $m$  according to magnetic activity.

Table 15L. Numerical expressions for the features of  $L$  after the removal of the oceanic dynamo effect.

	$D$	$H$	$Z$	$D+H$	$D+H+Z$
(a) Ratios of the range for $S$ to that for $L$					
all	17.6	4.9	10.5		
winter	8.4	2.1	7.6		
equinox	15.2	7.3	9.0		
summer	10.8	4.5	4.8		
(b) Ratios of the seasonal range to the annual mean range for $L$					
Winter/annual	$1.12 \pm 0.05$	$1.62 \pm 0.08$	$1.38 \pm 0.07$	$1.26 \pm 0.04$	$1.29 \pm 0.04$
equinox/annual	$1.26 \pm 0.07$	$0.94 \pm 0.07$	$1.35 \pm 0.07$	$1.10 \pm 0.05$	$1.18 \pm 0.04$
summer/annual	$2.40 \pm 0.08$	$1.38 \pm 0.07$	$2.62 \pm 0.11$	$1.82 \pm 0.05$	$1.97 \pm 0.05$
(c) Values of $10^4 m$ for the range of $L$					
all	$25 \pm 7$	$15 \pm 14$	$15 \pm 9$	$23 \pm 6$	$20 \pm 5$
(d) Values of $10^2 m'$ for the range of $L$					
all	$-44 \pm 8$	$-14 \pm 14$	$1 \pm 6$	$-37 \pm 7$	$-15 \pm 5$

one, especially for  $D$  and  $H$ . However, since the conductivity of the sea does not depend on seasons, sunspot number or magnetic activity, we might expect to find the same oceanic effect in each of the divisions according to these parameters. The cause of the observed variability of  $L_0$  between these divisions may be that the assumptions in the method to separate  $L_1$  and  $L_0$  from  $L_2$  do not necessarily hold good. The variability between seasons is partly due to the effect of the  $O_1$  component.

As shown in Fig. 26L, since the major part of  $L_2$  is  $L_1$  for  $D$  and  $H$ , the characteristics for  $D$  and  $H$  described in sections 5.1.–5.8. are generally unchanged and those for  $Z$  are somewhat changed when  $L_1$  takes the place of  $L_2$ . This is clear in Table 15L, which shows some numerical results corresponding to Tables 7L, 8L, 9L and 10L by replacing  $L_2$  with  $L_1$ . Comparing the results in the former with those in the latter, it is clear that there are no significant differences between them.

The results of the separation for Tables 3L, 4L, 5L and 6L are not given here, but the general characteristics are the same as those for Table 14L, with much more significant uncertainty.

**Acknowledgements:** The author wishes to thank Dr. M. Kawamura, Director of the Kakioka Magnetic Observatory, for his continuous support during this work. The author is very grateful to Prof. H. Maeda of Kyoto University and to Dr. K. Yanagihara, former Director of the Kakioka Magnetic Observatory, for their interest and encouragement. Almost all the computation for this work were carried out at the computer center of the Japan Meteorological Agency and the help given by the staff of the center is also gratefully acknowledged.

### References

- Chapman, S., The lunar and solar daily variations of the horizontal geomagnetic vector at Greenwich, 1848–1913, with an appendix on the lunar daily variation of magnetic declination at Pavlovsk and Sitka, *Abh. Akad. Wiss. Göttingen, Math. Phys. Kl.*, No. 3, pp. 72, 1957.
- Chapman, S. and B. Fogle, Solar and lunar daily geomagnetic variations at San Fernando and Greenwich in relation to the associated electric current systems, *Abh. Akad. Wiss. Göttingen, Math. Phys. Kl.*, No. 6, pp. 67, 1968.
- Chapman, S. and J. C. P. Miller, The statistical determination of lunar daily variation in geomagnetic and meteorological elements, *Month. Not. Roy. astr. Soc., Geophys. Suppl.*, 4, 649–669, 1940.
- Green, P. and S. R. C. Malin, Lunar and solar daily variations of the geomagnetic field at Watheroo, Western Australia, *J. Atmosph. Terr. Phys.*, 33, 305–318, 1971.
- Gupta, J. C., The solar and lunar daily geomagnetic variations at Sodankylä, 1914–1966, *Veröff. Geophys. Obs. Finn. Akad. Wiss.*, 56, 71–181, 1973.
- Leaton, B. R., S. R. Malin and H. F. Finch, The solar and luni-solar daily variation of the geomagnetic field at Greenwich and Abinger, 1916–1957, *Roy. Obs. Bull.*, No. 63, D273–D318, 1962.

- Malin, S. R. C., Separation of lunar daily geomagnetic variations into parts of ionospheric and oceanic origin, *Geophys. J. R. astr. Soc.*, **21**, 447–455, 1970.
- Malin, S. R. C. and S. Chapman, The determination of lunar daily geophysical variations by the Chapman-Miller method, *Geophys. J. R. astr. Soc.*, **19**, 15–35, 1970.
- Shiraki, M., Solar and lunar daily geomagnetic variations at Kakioka, Memambetsu and Kanoya, Japan, 1958–1973, *Geophys. Mag.*, **38**, (1), 37–70, 1977.
- Shiraki, M., Monthly mean lunar daily geomagnetic variations at Kakioka, Memambetsu and Kanoya, Japan, 1958–1973, *Geophys. Mag.*, **38**, (3), 59–72, 1978.
- Shiraki, M., On the lunar daily geomagnetic variations in Japan, submitted to *J. Geomag. Geoelectr.*
- Tschu, K. K., On the practical determination of lunar and luni-solar daily variations in certain geophysical data, *Aust. J. Sci. Res.*, **A2**, 1–24, 1949.

## 1913-1976 年の柿岡の地磁気太陰・太陽日変化

白 木 正 規

(地磁気観測所)

### 概 要

柿岡における1913-1976年(1917-1923年は欠測のため計57年間)の地磁気三成分の毎時値データを用いて、太陰・太陽日変化の解析を行った。データは、季節、太陽黒点数、地磁気活動度の三つのパラメータによって、計49個のグループに別けて、それぞれについて Chapman-Miller の方法で解析した。結果は、調和係数を表で示すと共に、デングラフ、ベクトルダイヤグラム、ハーモニックダイヤルで図示した。結果のいくつかの特徴点を記述し、議論した。